eprints@whiterose.ac.uk
https://eprints.whiterose.ac.uk/

Design and aerodynamic performance analyses of the self-starting H-type VAWT having J-shaped aerofoils considering various design parameters using CFD

Yunus Celik[a,b*], Derek Ingham[a], Lin Ma[a], Mohamed Pourkashanian[a]

[a] *Energy2050, Department of Mechanical Engineering, Faculty of Engineering, University of Sheffield, UK*

[b] *Department of Mechanical Engineering, Faculty of Engineering, Hakkari University, Turkey*

Abstract

Although the J-shaped aerofoil is a possible solution to enhance the torque generation at the low tip speed ratios, the effect of the J-shaped aerofoil on the overall and the dynamic start-up performances of the H-type VAWT has not been extensively studied. Therefore, for the first time, the present study is aimed at exploring the impact of the J-shaped aerofoil with different values of opening ratio on overall and dynamic start-up performance of the H-type VAWT considering different design parameters. The results show that a dynamic start-up model is needed to fully examine the self-starting capability of the J-shaped aerofoil instead of using calculated torque/power coefficients at the constant tip speed ratios. In addition, while the opening located at the inner surface of the aerofoil does not bring any benefit, the turbine self-starting ability increases with the increase in the opening ratio. Furthermore, there is a noticeable enhancement in the starting ability when the thicker NACA0018 aerofoil is employed, and the reversed version of the cambered aerofoils demonstrates a better self-starting capability compared to their original profiles. Additionally, the turbine with the J-shaped aerofoil having a slightly positive pitch angle ($\beta = 2°$) has been found to have a better self-starting ability.

Keywords

J-shaped aerofoil, Self-starting, Vertical axis wind turbine, Computational Fluid Dynamics (CFD), Aerodynamics

* Corresponding author. Hakkari University, Department of Mechanical Engineering, Faculty of Engineering, Hakkari, Turkey.

E-mail address: yunuscelik@hakkari.edu.tr

1. Introduction

The use of wind energy has increased rapidly in recent years, and it now plays a critical role in the production of renewable energy electricity. Wind turbines are often employed to extract the potential of the wind and can be mainly classified as horizontal axis wind turbines (HAWTs) and vertical axis wind turbines (VAWTs) [1]. Furthermore, there are two types of vertical axis wind turbines: the drag-driven Savonius rotor and the lift-driven Darrieus rotor [2]. Due to its higher power coefficient than VAWTs, HAWTs are widely used and currently dominate the field of large-scale wind power generation both on land and at sea [3].

Despite the fact that HAWTs are more advantageous than VAWTs from the maximum efficiency point of view when compared on the same scale, VAWTs have become a topic of investigation in recent years due to the inherent advantages that VAWTs have over HAWTs. These advantages can be listed as simple blade profile, omni-directional operation, affordable installation and maintenance cost, and lower noise, etc. [4]. On the other hand, apart from the advantages, VAWTs have several significant problems. The flow at the vicinity of the turbine is highly unsteady, which is because the azimuthal angle and angle of attack during the rotation are constantly changing. As a result of this, the turbine blades are exposed to all possible angles of attack during the complete rotation, making aerodynamic estimations more complex and difficult to comprehend [5].

Furthermore, the self-starting is also another major problem for the H-type VAWTs, especially for the ones that are used for the small-scale energy production. Unless the appropriate types of aerofoils, freestream wind speed, and turbine solidity are selected, H-type VAWTs may fail to self-start [6]. First and foremost, the understanding of the definition of self-starting is the first step to overcoming the self-starting problem of these turbines. Therefore, self-starting needs to be defined carefully. Although a Darrieus turbine is able to produce a small amount of forward torque when it is in a stationary condition, it may create a net torque per revolution at the initial starting stage, but it may then produce negative torque under certain circumstances over a range of tip speed ratio (λ) varying between about 0.5 and 2 depending on the blade geometry. Baker [7] describes this negative net torque region as the 'dead band'. According to his study, a turbine, which has this characteristic, may just start but it will not be able to escape this dead band in order to achieve its optimal working speed. Although various forms of the self-starting definition exist in the literature [8–10], in the present study, only if the turbine accelerates from rest to its final operating tip speed ratio, where the turbine has already passed the plateau stage, is it termed the self-starting [11].

The investigation of the self-starting behaviour of the Darrieus wind turbines, especially the H-type VAWT, has been a topic of intense conflict among the researches. In the literature, a number of

methods were proposed to overcome the self-starting problem of these turbines like pitching the blades, hybrid turbine designs, and optimising the turbine geometry including turbine solidity, blade thickness, and camber, etc. Although these methods may enhance the turbine self-starting capability, these can cause some of the major problems, such as a reduction in the final rotational speed at the steady-state condition and an efficiency loss in the peak power coefficient. Therefore, external electricity feed-in is generally needed to self-start the turbine. However, this external assistance results in much of this kind of turbine's advantages being lost.

Among all the possible solutions for the self-starting issue, the utilization of the different types of aerofoils in the H-type VAWT can significantly affect the turbine overall and self-starting performance. An optimum aerofoil profile of the H-type VAWT is expected to possess some desirable characteristics to obtain the optimum performance during the different turbine operating conditions, especially at the low tip speed ratios for the turbine self-starting ability. Therefore, a great number of numerical and experimental investigations on the impacts of the aerofoil profile on overall turbine performance and self-starting behaviour have been conducted [8,12–16]. However, as an alternative solution that can address the self-starting issue, the J-shaped profile has been applied to the VAWTs by a very small number of researchers. Chen et al. [17] investigated different surface opening ratios (the ratio of the cut-off length and the full aerofoil length) for the J-shaped aerofoil in order to overcome the issue of the self-starting of H-type VAWTs. Several opening ratios employed to the aerofoil surface were located on both the inner and outer sides of the turbine. The results show that in terms of the power performance at the optimum tip speed ratio and the starting torque generation, the desirable turbine can be obtained with the J-shaped aerofoil with 0.48 and 0.60 inner opening ratios while that of 0.72 and 0.84 outer opening ratios. Zamani et al. [18] studied a 3kW H-type VAWT by implementing the newly proposed J-shaped aerofoil profile. The main objective of this study was to enhance the starting torque of the H-type VAWT using the J-shaped profile. The findings indicate that the optimum turbine performance can be obtained using the J-shaped profile, which has the opening from the maximum thickness toward the trailing edge. More recently, Mohamed [19] criticised the J-shaped Darrieus type VAWT using different types of the aerofoils, such as NACA0015, NACA0021 and S1046, in terms of the turbine performance and noise generation. The author claims that the J-shape aerofoil decreased the turbine performance and did not reduce the turbine noise. However, this study was not carried out in accordance with the main purpose of J-shaped aerofoils. Because it is known that J-shaped aerofoils can increase the performance of the turbine at low λ values (generally less than 2) and decrease the performance at high λ values. However, the λ range investigated by the author was 2 to 5, but this range is not appropriate to evaluate the main purpose of J-shaped aerofoils.

1.1. Novelty and objectives

To make H-type VAWTs appropriate for small-scale energy production, the factors that hinder the turbine from self-starting should be thoroughly comprehended and developed to eliminate the problem. Therefore, the current study intends to provide a thorough investigation on the aerodynamic performance of the J-shaped aerofoil and to assist in the literature of J-shaped aerofoil research by conducting detailed analyses on the influence of the various design parameters including opening design, blade shape, pitch angle, etc.

The main gaps identified in the literature of the J-shaped aerofoil for H-type VAWTs are briefed as follows:

- The aerodynamic performance of the J-shaped aerofoil is not fully understood due to the inconsistent results obtained in the previous studies and the lack of detailed studies addressing its importance in terms of the aerodynamics.

- None of studies in the literature investigated the turbine self-starting behaviour considering the dynamic start-up data. In the previous studies, the self-starting performance of the H-type VAWT having a J-shaped aerofoil was assessed based on the calculated torque coefficient or power coefficient at the particular low λ values, which only implies whether the turbine may self-start or not and never provides a deeper knowledge of the effect of the J-shaped profiles on the turbine dynamic self-starting behaviour.

- Analysis of the impact of the most influential design parameters, such as aerofoil profile and blade pitching, on the turbine self-starting performance when a J-shaped aerofoil is used, meaning that the very important recommendations to obtain a design of the H-type VAWT having an optimum J-shaped aerofoil configuration can be provided.

To address the gaps defined above, the present study has the following aims and objectives:

- Build and employ a method that is based on the time-varying start-up data for a thorough analysis of the aerodynamic behaviour of the J-shaped aerofoil in comparison with its conventional profile when it is employed for VAWT.

- Investigate the effect of the openings located on the aerofoil outer and inner surfaces on the self-start of the turbine.

- Investigate the influence of the J-shaped aerofoil with the different opening ratios on the turbine torque generation considering the low and high λ values.

- Provide extensive knowledge of the lift and drag contributions of the J-shaped profile to the torque generation at different λ values.

- Evaluate a number of aerofoil profiles with and without an opening for the dynamic start-up performance of the turbine.

- Examine the impact of the pitch angle on the turbine self-starting performance using the J-shaped aerofoils in comparison with the conventional aerofoil.

2. Method description

Several fixed rotational speeds for the rotor are defined in the traditional approach of CFD analysis of VAWT, and the torque is determined for each rotational speed. However, in the present study, a method based on the interaction of the fluid and turbine has been employed. In this method, the solution starts where the turbine is at rest and the instantaneous aerodynamic torque (T_w) corresponding to the turbine instantaneous position can be calculated using Eq.1 depending on the aerodynamic lift force (F_l) and drag force (F_d) that are obtained through the solution of the Navier-Stokes equations.

$$T_w = \sum_{i=1}^{3}(F_l sin\alpha - F_d cos\alpha) \times R)_i \tag{1}$$

In the next time step, the acceleration the turbine (a) can be obtained by using the equation of motion (Eq.2) taking into consideration the moment of inertia (I) and the resistive torque (T_{res}) (if available).

$$a = \frac{T_w - T_{res}}{I} \tag{2}$$

Once the acceleration of the turbine is found, the new rotational speed (ω_{t+1}) and new azimuthal position (θ_{t+1}) of the turbine for the next time step can be also obtained using the Eq.3 and Eq.4.

$$\omega_{t+1} = \omega_t + a\Delta t \tag{3}$$

$$\theta_{t+1} = \theta_t + \omega_{t+1}\Delta t \tag{4}$$

This procedure will be repeated to calculate the new aerodynamic forces and the new rotational speed for the next time step and continued until the turbine reaches its final rotational speed at the steady-state condition. According to this procedure, the 6 degrees of freedom (6DOF) user-defined function (UDF), which consists of the turbine moment of inertia and its other physical characteristics, were written in the C language and employed in the dynamic mesh zone section of ANSYS Fluent solver. A typical example of the UDF code used in the 2D CFD start-up simulations is provided in the Appendix. However, although the moment of inertia for the turbine was stated

as 0.018 kgm^2 in the experimental configuration [20], the moment of inertia was recalculated for the 2D CFD simulations by considering the height of the turbine as 1m, instead of 0.6m (in the experiment). The newfound value for the inertia was 0.03 and it is consistent with [21,22].

3. CFD simulation process

3.1. Model description and computational settings

The CFD can be applied to the VAWT simulations due to their ease and accurate predictions compared to the other types of methods such as the Blade Element Momentum model [11]. Since the previous studies [23–30] have illustrated that 2D CFD models can yield acceptable results while effectively revealing the most critical factors that influence the overall performance of the turbine and the flow physics at the vicinity of the turbine blades, a 2D CFD model has been created and employed to analyse the aerodynamic performance of the H-type VAWT in the present work.

Due to a limited number of studies existing in the literature related to turbine self-starting, a published experimental study conducted by Rainbird [20] was selected for the validation purpose of the current CFD dynamic start-up model. Instead of the simply calculated overall torque/power coefficients, a time-varying behaviour of the turbine self-starting data has been computed in the experiment, and this provides a good opportunity for the validation of the present 2D CFD dynamic start-up model. In the current study, the main configuration of the investigated H-type VAWT has been selected according to the experimental setup. The turbine has a diameter of 0.75m with three NACA0018 aerofoils having a chord length of 0.083m. The CFD model that will be employed in the investigations was created using the ANSYS Design Modeller, and Table 1 shows the main features of the wind turbine.

Table 1. The main features of the wind turbine used in the present study.

Description	Value	Unit
Number of blades	3	-
Chord length	0.083	m
Span height	0.6	m
Diameter of turbine	0.75	m
Blade profile	NACA0018	-
Turbine moment of inertia	0.3	kgm²

Semi-Implicit Method for Pressure Linked Equations (SIMPLE), a pressure-velocity coupling algorithm that enforces mass conservation by using a relationship between velocity and pressure corrections, was employed in the simulations with the node-based gradient that is known as the

Green-Gauss Node Based [31]. The second-order upwind scheme that provides a better balance between accuracy and robustness is used for the temporal and spatial discretization of the convection terms of the momentum and turbulence model equations [23]. The simulations were run with various numbers of iterations and magnitudes of the convergence criteria to evaluate the sensitivity of the results in regards to the number of iterations and residual convergence criteria. It was discovered that at least 25 iterations are required to obtain all scaled residuals $< 1 \times 10^{-5}$, which agrees with previous research [32]. Since the turbulent intensity of the wind tunnel in the experiment was unknown, a sensitivity study was performed to determine the proper turbulent intensity and viscosity ratio, which were determined to be 1% and 10, respectively. All simulations have been run on the University of Sheffield's HPC (High-Performance Computing) facilities with double precisions, and when 16 cores were employed, each simulation took at least 9 hours to complete.

Furthermore, because of the complex flow structures at the vicinity of the VAWT, a proper selection of the turbulence model is a crucial part of the CFD simulations, especially at the low λ regions. In this regard, it can be observed in the literature that the two-equation turbulence models, such as $k-\varepsilon$ and $k-\omega$, are widely employed in the wind turbine analyses, and one of the $k-\omega$ turbulence model, which is the Shear Stress Transport (SST) $k-\omega$ model has become more popular for VAWT simulations [33]. The SST $k-\omega$ turbulence model has been proposed as a hybrid model that combines the $k-\omega$ and $k-\varepsilon$ models. While the $k-\omega$ model is employed for the near wall region, the $k-\varepsilon$ is used for the regions that are away from the wall [34]. Although the $k-\omega$ models need to be meshed well in order to analyse the flow near the wall that may result in the method being much more expensive compared to the $k-\varepsilon$ model, it provides more reliable results. For this reason, the SST $k-\omega$ turbulence model is widely employed in many CFD simulations by researchers [15,35–41]. Consequently, the SST $k-\omega$ turbulence model has been selected for the turbulence modelling in the model verification studies and further investigations.

3.2. Model verification

In this section, sensitivity analyses were carried out in order to achieve a precise CFD model, and then the predicted result and the experimental data have been compared to be sure of the reliability of the present 2D CFD model. The computations with various domain sizes, grid resolutions, and time-step sizes have been analysed to ensure the independent of the results on these parameters. Two tip speed ratios (λ), namely (λ=1.5) and (λ=3) have been selected for the sensitivity studies in order to ensure that the selected parameters in this study can produce the consistent results at both low and high tip speed ratios.

The computational domain consists of two zones, namely the rotating domain and the stationary domain, which has been created in ANSYS Design Modeller. The two zones are coupled using interface boundary conditions in order to ensure that the continuity in the flow field is formed. The constant freestream velocity, which is perpendicular to the inlet, is defined as $V_\infty = 6m/s$ based on the experimental data [20]. The Reynolds number corresponding to the freestream wind velocity used in the experiment varies between 0 and around 1.1×10^5 since the turbine rotational speed varies, starting from rest and accelerating until the steady-state condition is reached. Under these circumstances, the turbine can be considered as working in the urban environment conditions where the fluid flow around the turbine becomes incompressible and laminar-to-turbulent transition [42,43]. Therefore, an appropriate turbulence model, SST $k-\omega$, that effectively covers these transitional flows and to calculate the aerodynamic loads has been selected. In addition, the outlet is set as a zero-gauge pressure outlet and the no-slip condition is applied to the blade surfaces. The top and bottom sides of the computational domain are assumed as the symmetry boundary conditions to minimize the effect of the blockage [44].

Three different domain sizes, namely Domain 1, Domain 2, and Domain 3, which have the dimensions of (30R length × 12R width), (40R length × 16R width), and (50R length × 20R width), respectively, have been investigated at both low values of λ of 1.5 and high λ of 3 to analyse the influence of the domain size on the simulation results. The comparison of the torque coefficients for the domain sizes investigated at both tip speed ratios is demonstrated in Fig. 1. It has been found that the Domain 2 can be selected as the final computational domain due to the values indicated in the Fig. 2 for the model validation study and further investigations. The reason for choosing the Domain 2 is that the discrepancy between the Domain 2 and Domain 3 for both tip speed ratios is very slight. In addition, the final dimensions of the computational size is in good agreement with the other relevant literature [45,46].
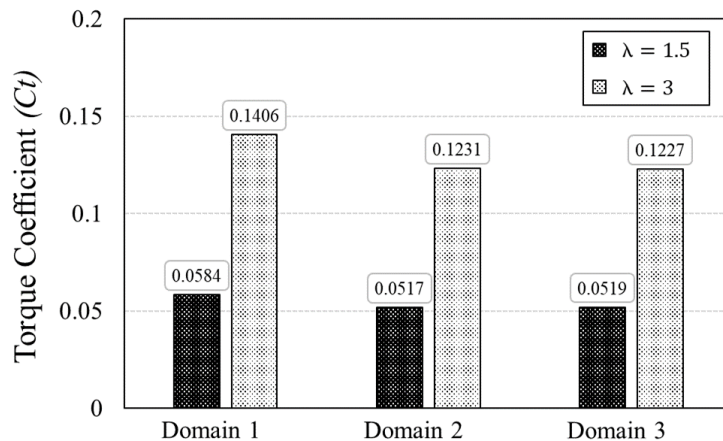

Fig. 1. Comparison of the torque coefficient for the different domain sizes at λ=1.5 and λ=3.
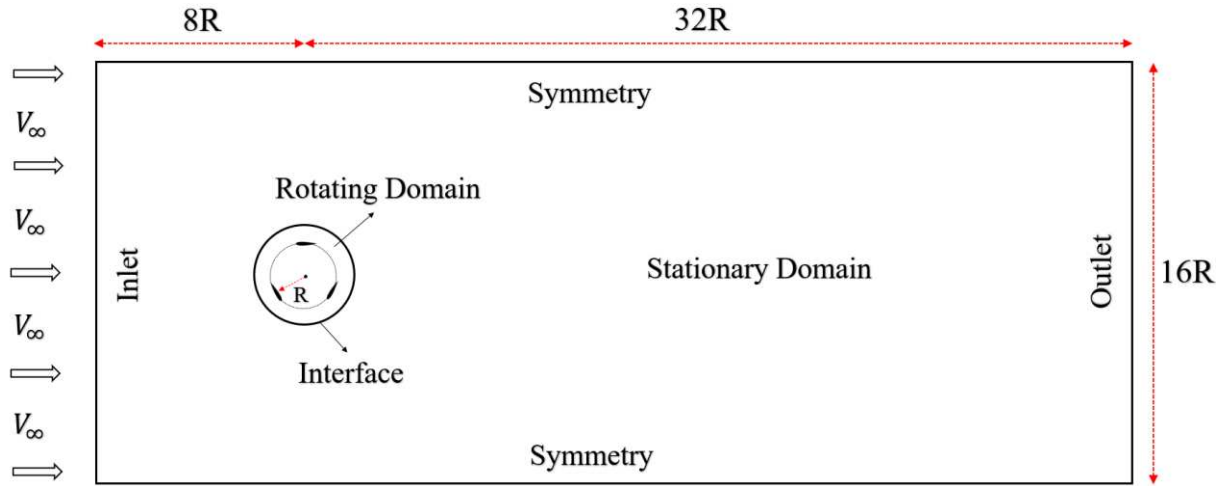
Fig. 2. 2D computational domain of the current study and boundary conditions (note sketches are not in scale).

Furthermore, based on the recommendations of Almohammadi et al. [47], a hybrid mesh has been selected to generate the computational grid due to the most advantageous type for reducing the number of mesh elements in the computational domain. The selected hybrid mesh in this study comprises a structured mesh applied to both the vicinity of aerofoils and the stationary domain, while an unstructured mesh has been applied to the rotating domain, as shown in Fig. 3. In addition, 15 mesh layers of the quadrilateral elements with the first layer height of about 0.02 mm is utilised to resolve the viscous sub-layer [48]. Thus, a dimensionless y^+ value having an average wall distance $y^+ < 1$ with a maximum value of 2.5 has been obtained throughout the simulations, which assists in accurately estimating the aerodynamic forces acting on the turbine blade [27]. To achieve an optimum number of nodes surrounding the aerofoil, three different number of nodes, namely Node 1, Node 2, and Node 3 that have 800, 1000, and 1200 nodes, respectively, were examined. The mesh intensity for the far field regions, such as the stationary domain, has been refined enough in order to reduce its impact on the results and while changing the number of nodes around the aerofoil, the mesh element numbers in these regions are kept constant throughout the mesh independence analysis. Fig. 4 demonstrates a comparison of the torque coefficients for the different number of nodes, in the vicinity of the aerofoil, at two different λ values, such as λ=1.5 and λ=3. As observed in Fig. 4, even though there is a negligible difference observed between the nodes investigated at λ=3, only a small discrepancy was obtained between Node 2 and Node 3 while Node 1 is quite different at λ=1.5. Therefore, the present mesh independency study findings suggest that Node 2, which has 1000 nodes around the aerofoil, is the best node to be used based on the accuracy and computational efficiency. Thus, the total number of nodes for the mesh structure that would be employed in future investigations was found to be around 204,000 in the whole domain. The average skewness that is achieved has a value of 0.102 and with a maximum of 0.655. Since a

skewness higher than 0.95 illustrates a very poor quality of the meshing [49], then the maximum value of the skewness of 0.655 that occurs in a small fraction of the computational domain (only in 6 cells) in the present study indicates that the mesh quality is sufficient. Furthermore, the average orthogonal quality obtained in the present grid is 0.961 and with a minimum value of 0.71. Consequently, the present mesh demonstrates the excellent quality and it is consistent with the previously published studies [25,50].
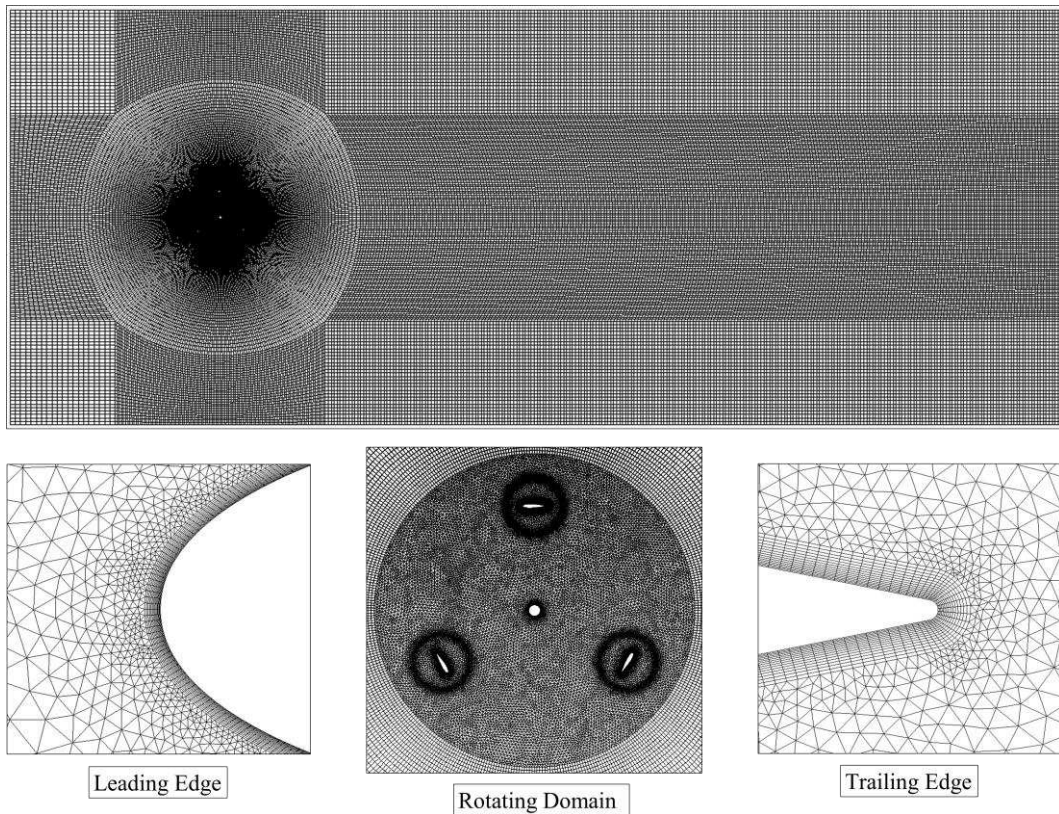

Fig. 3. Grid details of the computational domain including the rotating domain, and the leading and trailing edges.
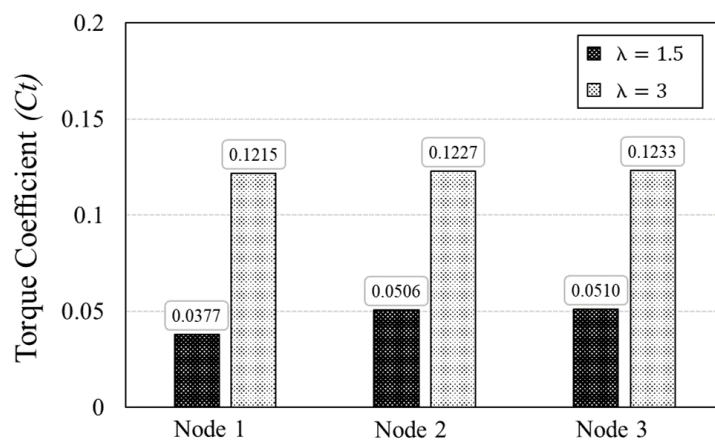

Fig. 4. Comparison of the torque coefficient for the different number nodes surrounding the aerofoil at λ=1.5 and λ=3.

Three different time steps, $\Delta t1 = 0.00144s, \Delta t2 = 0.00072s,$ and $\Delta t3 = 0.00036s,$ have been evaluated for the time step size independency study at both λ values of 1.5 and 3 and compared in terms of the torque coefficient, as shown in Fig 5. Due to the insignificant difference obtained between $\Delta t2$ and $\Delta t3$ at both λ values, the time step size of $\Delta t2 = 0.00072s$ was found to be the best time step to be used based on the accuracy and computational efficiency. Since the present self-starting simulations are based on the time-varying data, which is in contrast to the conventional method that is based on the constant rotational speed, the selected time step size for the present investigations correspond to the varying azimuthal increments at different operating conditions. For instance, at λ=0.5, the azimuthal increment is found to be around 0.33 degree, while it is about 2.31 degree at λ=3.5. The selected time step size is in good agreement with the previous findings [51,52]. Furthermore, the value of the Courant number, which is related to the time step size, is recommended to be less than 40 during the simulations for complex unsteady flows [53]. In the present study, the Courant number has been found to have a maximum value of 10, and this is a value that is consistent with the value employed in the existing literature [43,53].
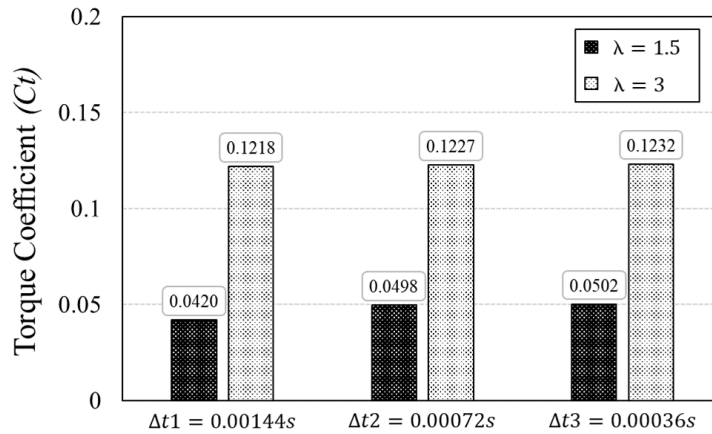

Fig. 5. Comparison of the torque coefficient for the different time step sizes at λ=1.5 and λ=3.

After the sensitivity studies, the final obtained 2D CFD start-up model was compared with the experimental data provided by Rainbird [20] in Fig. 6. In order to make it easier to observe the comparison between the current result and experimental data, the non-dimensional time axis defined as t/T (T is the time when the turbine reaches the steady-state condition) has been employed. The turbine used in the experiment reaches steady-state condition at a tip speed ratio of roughly 3.2, whereas this tip speed ratio has been found to be 4.1 in the present CFD model (see Fig. 6).
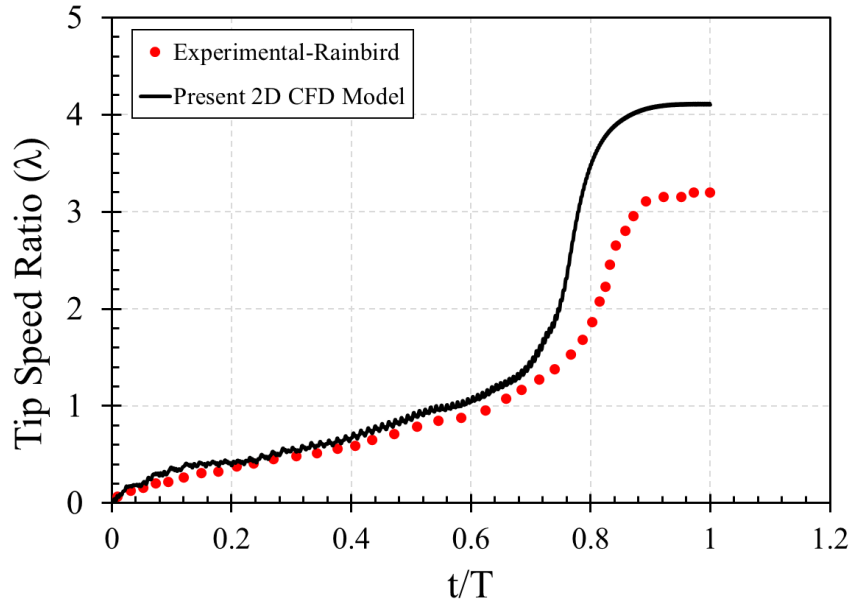
Fig. 6. Variation of the tip speed ratio with the normalized time for the comparison between the present 2D CFD and the experimental results.

The discrepancy between the simulated and experimental results, especially at the high tip speed ratios, could be attributable to the following:

- The presence of 3D effects, namely the tip losses and the blade supporting arms and that are not considered in the present 2D CFD model [21].

- Other sources of the resistive torque, such as generator losses and bearing friction, can lead to the observed over-prediction when compared to the experimental data [54]. However, the resistive torque impact on the self-starting behaviour has not been included in the present CFD simulations because of the lack of information presented in the experimental data.

- The uncertainties associated with the experimental study, for instance the blade-spoke connection, are not explicitly stated in the experiment data [20]. It is known that the influence of the blade-spoke connection on the power performance of the turbine more severe at higher λ values [4]. This might explain the higher divergence between the experimental data and the numerically predicted rotational speed by the present CFD model, notably during the acceleration period and steady-state condition.

Although a noticeable difference between the numerical prediction and experimental data is observed in the high tip speed ratio areas, the results for the critical tip speed ratio range, $0 < \lambda < 1$, are in good agreement. The current finding is also consistent with the existing previous studies in the literature [21,51,52]. Consequently, the obtained 2D CFD model has been found to be sufficient for the accurate investigation for the further studies of the self-starting characteristics of the H-type VAWTs having different configurations of the J-shaped aerofoils.

4. Results and discussions

As observed in the previous section, the research turbine used in the validation study is able to escape the plateau stage and reach its steady-state operating condition under the freestream wind speed of $V_\infty = 6m/s$. However, a series of preliminary numerical studies has been conducted to assess the turbine net torque generation at different λ values and if the turbine will be able to self-start under freestream wind speeds lower than $6\ m/s$, i.e. 4 and $5m/s$. The purpose of examining different freestream wind speed conditions is to determine the problematic turbine and to overcome the self-starting deficiency of the turbine by employing the J-shaped aerofoil.

Firstly, the turbine performance has been analysed at eight constant tip speed ratios in terms of the generated net torque. Fig. 7 illustrates the comparison of the turbine torque coefficients at various tip speed ratios for different freestream wind speeds. There are two distinct regions observed in this figure: (i) with the free wind speed lower than $6m/s$, the turbine generates a net negative torque region at low λ values, known as "the dead band" [7]. This negative torque region may prevent the turbine speed up and escape from the plateau stage unless this dead band is sufficiently small, and the turbine can gain enough momentum to break through the plateau stage. Therefore, it can be expected that the turbine under the freestream wind speeds $4m/s$ and $5m/s$ may fail to self-start. (ii) Considering the optimum tip speed ratio, where the turbine produces the higher torque, the magnitude of the torque generated increases with the increase in the wind speed.
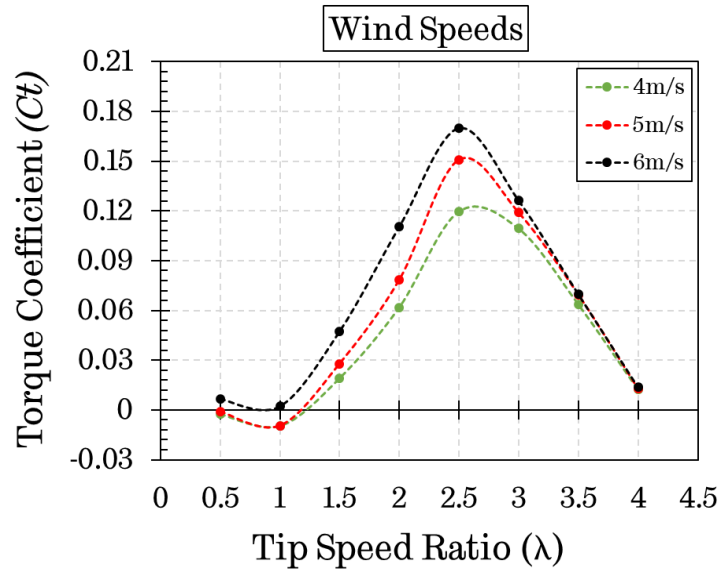

Fig. 7. Variation of the torque coefficient with the tip speed ratio for different freestream wind speeds of $V_\infty = 4, 5, 6m/s$.

Secondly, a further study has been conducted by investigating the turbine dynamic start-up behaviour under different freestream wind speeds as shown in Fig. 8. The turbine can only self-start at a freestream wind speed of $6m/s$, as shown in the figure. This finding supports the results obtained in the turbine torque coefficient versus tip speed ratio curve (see Fig. 7), which showed no dead band under the freestream wind speed of $6m/s$.

Since the results obtained in the present section illustrates that the turbine is not able to self-start under the freestream wind speeds lower than $6m/s$, a freestream wind speed of $5m/s$ has been selected for further investigations to analyse the capability of the J-shaped aerofoil on the improvement of the self-starting ability of the H-type VAWTs.
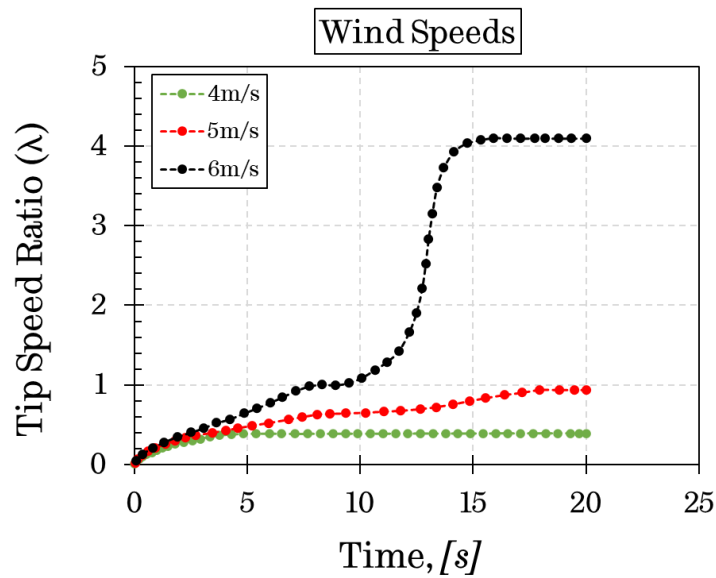

Fig. 8. Variation of the tip speed ratio with the time for different freestream wind speeds of $V_\infty = 4, 5, 6m/s$.

4.1. Self-starting performance analyses of the J-shaped aerofoils

The present section has been designed to evaluate the turbine with the J-shaped aerofoils with different numbers of the opening ratios, in terms of the performance at low and high λ values, and the dynamic start-up behaviour under the freestream wind speed of $V_\infty = 5m/s$. The same turbine features were studied as in the validation study, i.e., with a conventional aerofoil NACA0018, the turbine radius of $R = 0.375m$ and the blade chord length of $c = 0.083m$. Six opening ratios, 10%, 20%, 30%, 40%, 60%, and 90%, located at the outer and inner surface of the aerofoil have been investigated. The schematic of the turbine with the original NACA0018 aerofoil profile (no cutting) and the aerofoils with six different opening ratios (OR) are investigated when the openings are located at the outer surface have been illustrated in Fig. 9.
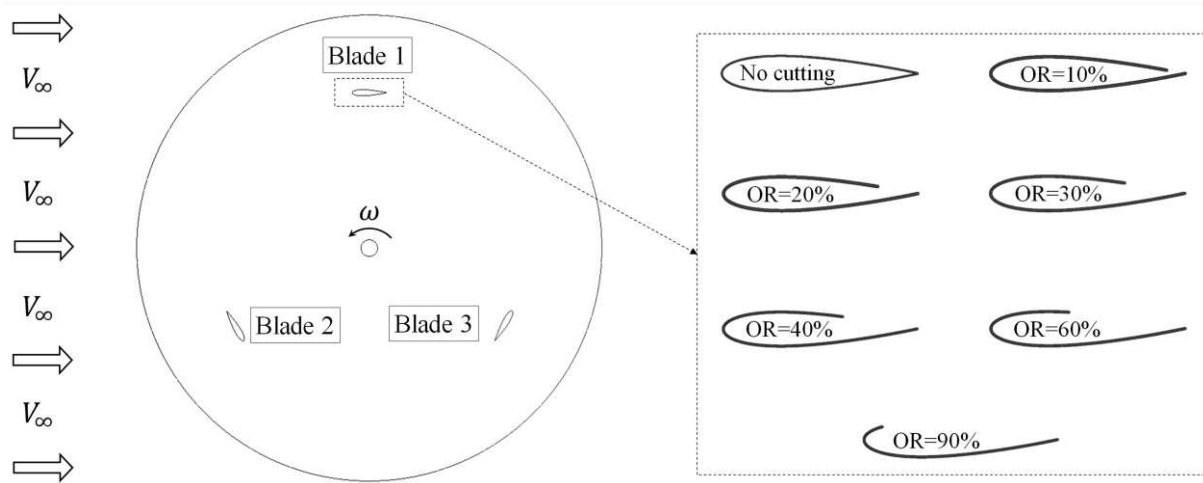
Fig. 9. The schematic of the turbine and the aerofoils with six different opening ratios, namely 10%, 20%, 30%, 40%, 60%, and 90%.

4.1.1. Influence of the opening locations

In this part of the study, the effect of the opening location on the turbine dynamic start-up behaviour have been investigated for the J-shaped aerofoils with the different opening ratios. Firstly, the J-shaped aerofoil with the openings located at the outer surface has been considered. Fig. 10 demonstrates the variation of the turbine tip speed ratio with the time for the turbine having the J-shaped aerofoil with different opening ratios considering the openings located at the outer surface. As can be observed in the figure, with the increase in the opening ratio, the start-up time reduces, while the tip speed ratio at the final steady-state decreases. However, the turbine with the original aerofoil profile and the J-shaped aerofoil with a 10% opening ratio cannot escape the plateau stage and fail to start. It is suggested that the reason that caused this situation is as a result of the negative torque generated at the critical tip speed ratio range, which is the tip speed ratio less than 1.
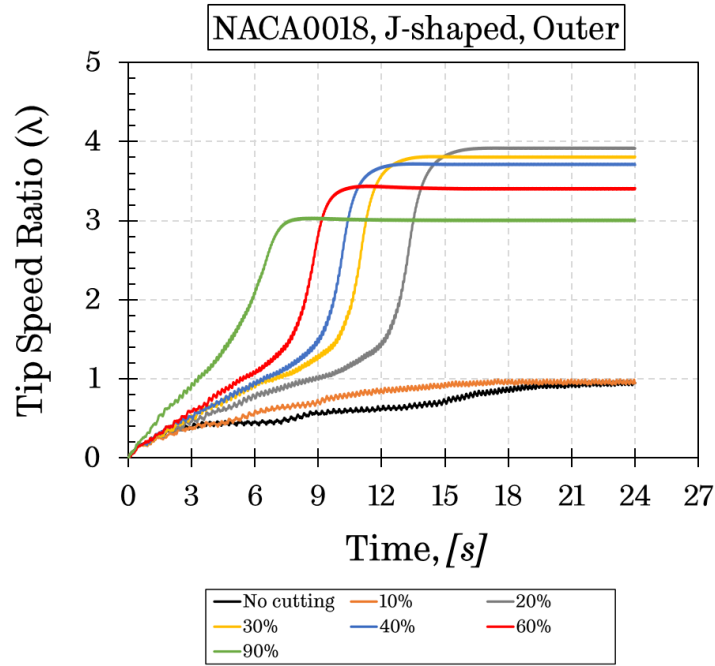
Fig. 10. Variation of the tip speed ratio with the time for the turbine having the J-shaped aerofoils with different openings located at the outer surface.

Furthermore, in order to fully understand the effect of the opening ratio on the turbine dynamic start-up behaviour, the J-shaped aerofoils with the openings located at the inner surface have been also investigated. Fig. 11 presents the variation of the tip speed ratio with the time for the turbine having the J-shaped aerofoils with different openings located at the inner surface. Clearly, the turbine with the J-shaped aerofoil with the larger and smaller openings do not provide the self-starting ability, but the opening ratios of 30-40% do assist the turbine to self-start and they reach the same final speed as when the opening is in the outer side but take a much longer time.
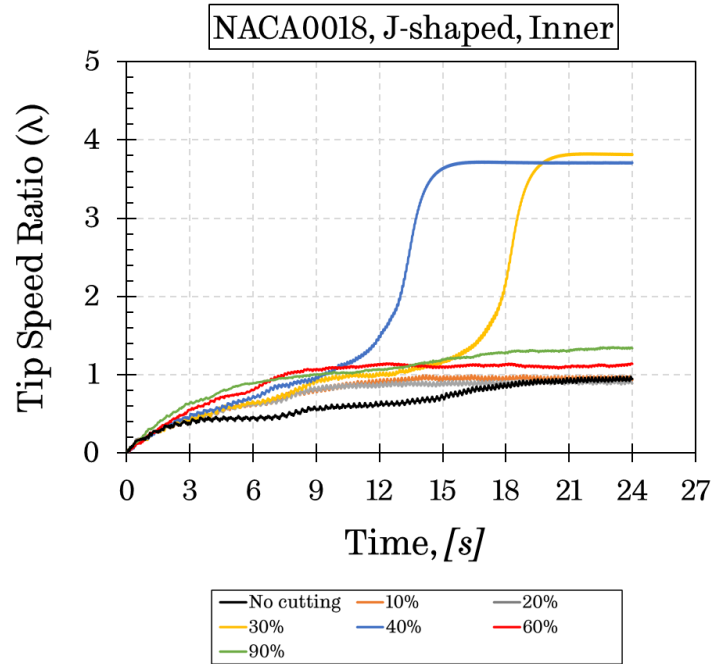
Fig. 11. Variation of the tip speed ratio with the time for the turbine having J-shaped aerofoils with different openings located at the inner surface.

It can be concluded that the turbine with the J-shaped aerofoil with the openings located at the inner surface does not appear to bring any benefit and makes the choice of the inner profiles unreasonable compared with the outer surface. For this reason, the J-shaped aerofoil with the openings located at the outer surface will be employed in the further investigations.

4.1.2. The effect of the opening ratios on the turbine torque generation

The turbine torque coefficient at several tip speed ratios considering the different openings has been analysed under the freestream wind speed of $5m/s$ for the outer surface opening. For this purpose, four λ values, such as λ=0.5, λ=1, λ=2.5, and λ=3.5, which are corresponding to the low λ and relatively high λ, have been selected in order to demonstrate the effect of the J-shaped aerofoils under various turbine operating conditions. The torque coefficients obtained at the selected λ values have been presented in Fig. 12 as a function of the tip speed ratio. The figure illustrates that the J-shaped aerofoil with different opening ratios shows different aerodynamic characteristics at low and relatively high λ regions. Therefore, in order to provide a comprehensive understanding of the influence of the J-shaped profile with different opening ratios on the turbine torque generation, the low and high λ regions should be evaluated separately.
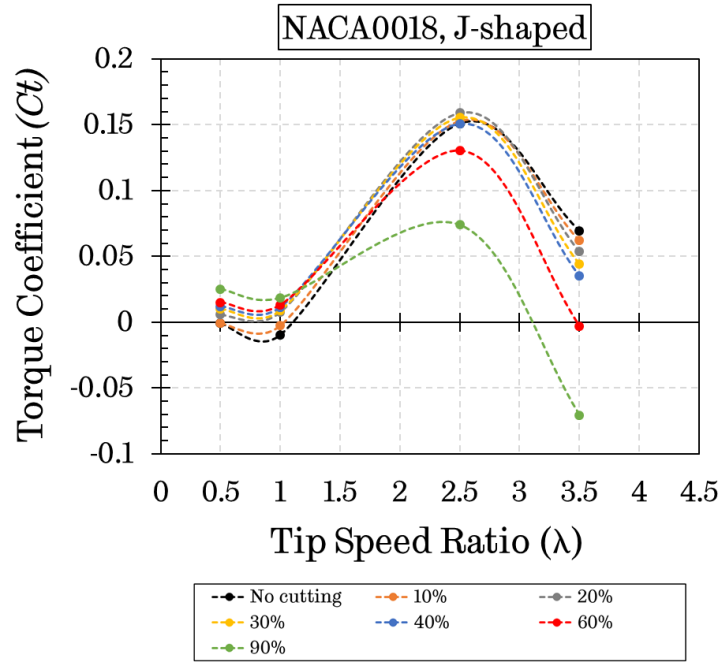
Fig. 12. Variation of the torque coefficient with the tip speed ratio for different opening ratios.

At the low λ region in which $\lambda = 0.5$ and $\lambda = 1$, the turbine with the original aerofoil (no cutting) and 10% opening ratio produces negative torque, which results in the failing to self-start, as shown in Fig. 12. On the other hand, the generated torque increases with the increase in the opening ratio, but the one with a 90% opening ratio has a noticeably larger amplitude at both investigated λ values, which is beneficial to the turbine self-starting ability. It is also observed that increasing the torque coefficients at the low λ values are not linear with respect to the increasing in the opening ratios.

Further investigations on the variation on the instantaneous torque coefficient of a single blade with the azimuthal angle for different opening ratios when $\lambda = 0.5$ and $\lambda = 1$ have been plotted in Fig. 13. This investigation provides more specific information on the effect of the opening ratios regarding the upstream and downstream part of the turbine to further understand the instantaneous torque loss caused by the opening. Although there is no clear difference observed between the J-shaped aerofoils with different openings in the downstream part ($180° < \theta < 360°$) of the turbine, the instantaneous torque coefficient appears to increase with the increase in the opening ratio in the upstream part ($0° < \theta < 180°$) of the turbine at both tip speed ratios investigated. That is the reason why the turbine with the J-shaped aerofoil with a larger opening ratio produces a much greater torque than the turbine with the smaller opening ratios at these tip speed ratios (see Fig. 12).
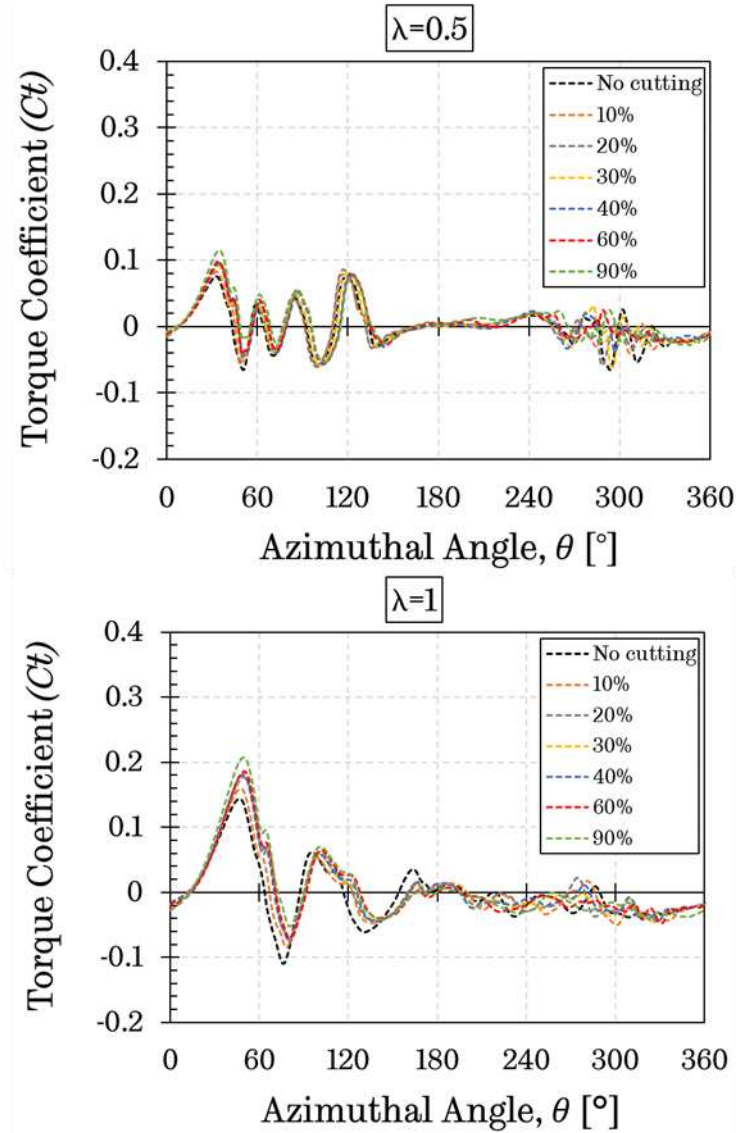
Fig. 13. Variation of the instantaneous torque coefficient with the azimuthal angle for different opening ratios at λ = 0.5 and λ = 1.

Furthermore, at the relatively high λ region in which λ = 2.5 and λ = 3.5 (see Fig. 12), the J-shaped aerofoil demonstrates different aerodynamic behaviour. At λ = 3.5, the turbine torque coefficient gradually decreases with the increase in the opening ratios. The result of this investigation shows that although the increasing opening ratio increases the possibility of the turbine self-starting, due to the generated high torque at the low λ values, it may cause a large penalty on the generated torque at the high tip speed ratios. On the contrary, at the optimum tip speed ratio of λ = 2.5, where the turbine generates a highest torque, the turbine with the J-shaped aerofoil with a 20% opening ratio generates the highest torque coefficient compared to the other cases. The reason behind this situation might be explained by looking at the aerodynamic behaviour of the turbines investigated. Therefore, a comparison between the different opening ratios in terms

of the lift and drag coefficients has been presented in Fig. 14 at λ = 2.5. As it can be seen in the figure, even though there is no significant difference observed in the downstream part of the turbine, except the 90% opening ratio, the lift coefficient increases with the increase in the opening ratios in the upstream part of the turbine. On the contrary, it is clear that the drag coefficient increases with the increase in the opening ratios in both the upstream and downstream part of the turbine, which causes a significant reduction on the overall performance.
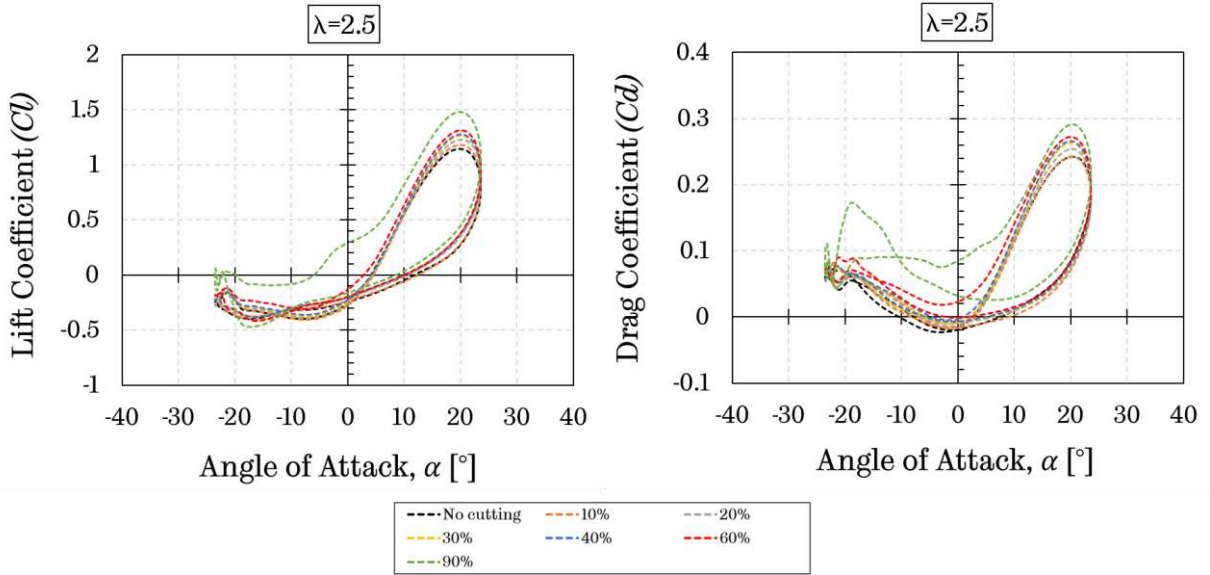

Fig. 14. Variation of the lift and drag coefficients with the angle of attack for the different opening ratios at λ = 2.5.

A further comparison between the J-shaped aerofoil with the original profile and a 20% opening ratio in terms of the lift and drag force coefficients has been presented in Fig. 15 in order to better understand why the turbine with the J-shaped aerofoil with a 20% opening ratio produces a higher torque coefficient compared to the original profile. As it can be seen in the figure, although both aerofoils exhibit a similar pattern in the lift coefficient in the downstream part of the turbine, the J-shaped aerofoil with 20% opening ratio generates a greater lift force coefficient than that of the original profile at almost all the angles of attacks in the upstream part of the turbine. In contrast, regarding the drag force coefficient in the positive angles of attack region, the J-shaped aerofoil procures a higher drag in the region where the angle of attack increases from 0° to the maximum angle of attack (23.57°) while the original profile generates a higher drag in the region where the angle of attack decreases from the maximum angle of attack (23.57°) to 0°. This leads to a similar drag force generation in the upstream part of the turbine. This is the reason why the turbine with J-shaped profile with a 20% opening ratio produces a slightly higher torque coefficient compared to the original aerofoil profile at the λ = 2.5.
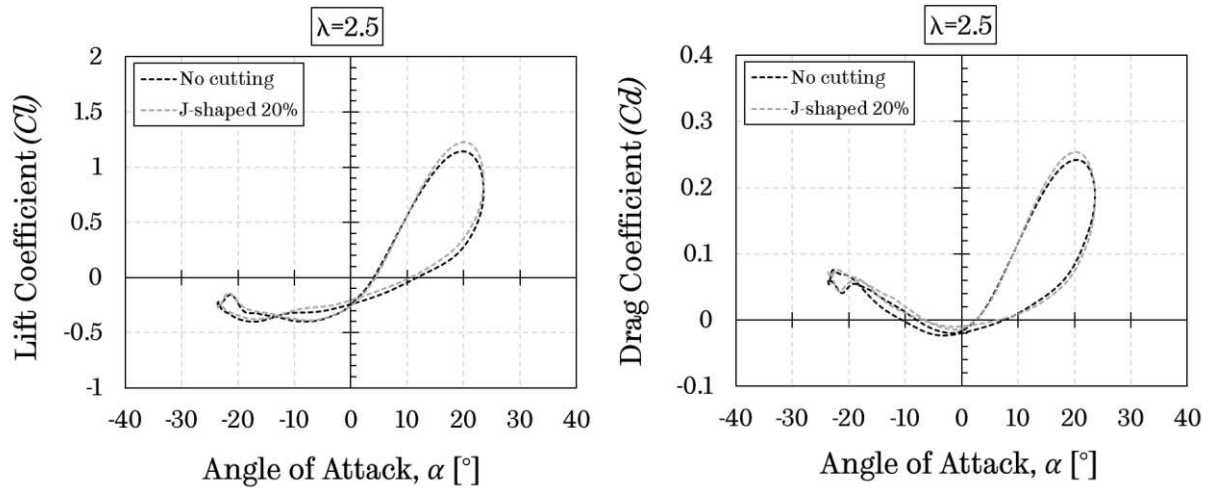
Fig. 15. Comparison between the J-shaped aerofoil with the original profile (no cutting) and a 20% opening ratio considering the lift coefficient and drag force coefficient at λ = 2.5.

To further explore the loss of overall efficiency at the high λ values when the J-shaped aerofoils are employed, the variation of the blade instantaneous torque coefficients with the azimuthal angle for the aerofoils investigated at λ = 2.5 and λ = 3.5 have been illustrated in Fig. 16. At λ = 2.5, although the magnitude of the instantaneous torque coefficient increases with the increase in the opening ratio in the upstream part of the turbine, the loss of the instantaneous torque coefficient significantly increases along the entire downstream part of the turbine when the opening ratio increases. However, at λ = 3.5, the difference on the instantaneous torque coefficients generated by the aerofoils investigated in the upstream part of the turbine decreased, but the J-shaped aerofoil with a 90% opening still produces a much greater torque coefficient at the azimuthal position between 60° and 150°. Conversely, regarding the downstream part of the turbine, the blade instantaneous torque coefficient significantly decreases with the increase in the opening ratio. Therefore, this is the reason why the turbine with the original aerofoil profile is able to produce a much greater torque at the high tip speed ratio regions.
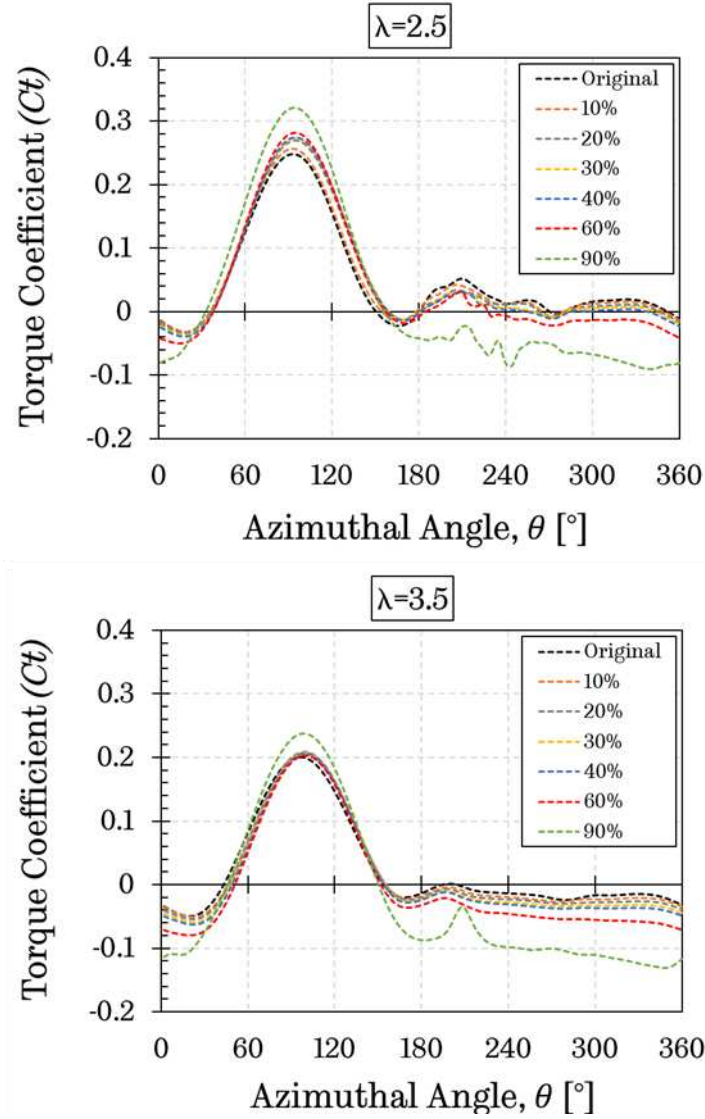
Fig. 16. Variation of the instantaneous torque coefficient with the azimuthal angle for different opening ratios at λ = 2.5 and λ = 3.5.

Fig. 17 shows the pressure coefficient contours at the vicinity of the aerofoils at different positions for the original aerofoil and its J-shaped profiles with 40% and 90% opening ratios. These contours have been obtained at the tip speed ratios of 1 and 2.5. Since the pressure distribution over the pressure and suction sides of the investigated aerofoils demonstrate the similar characteristics at λ=1, the instantaneous torque coefficients produced by the aerofoils investigated in both upstream and downstream parts of the turbine (at the azimuthal angle of 120° and 240°) have a similar value (see Fig. 13). However, at λ=2.5, in the upstream part of the turbine (θ = 120°), the pressure difference between the pressure and suction sides of the aerofoils increases with the increase in the opening ratio, which leads to a higher instantaneous torque coefficient for the turbine with a 90% opening ratio. Furthermore, at λ=2.5, in the downstream part of the turbine (θ = 240°), this pressure difference decreases with the increase in the opening ratio, which results in a lower, even

22

negative instantaneous torque generation (see Fig. 16). Due to the higher amount of negative torque generated at the downstream part of the turbine when the largest opening employed (90%), the overall turbine torque generation dramatically decreases (see Fig. 12).
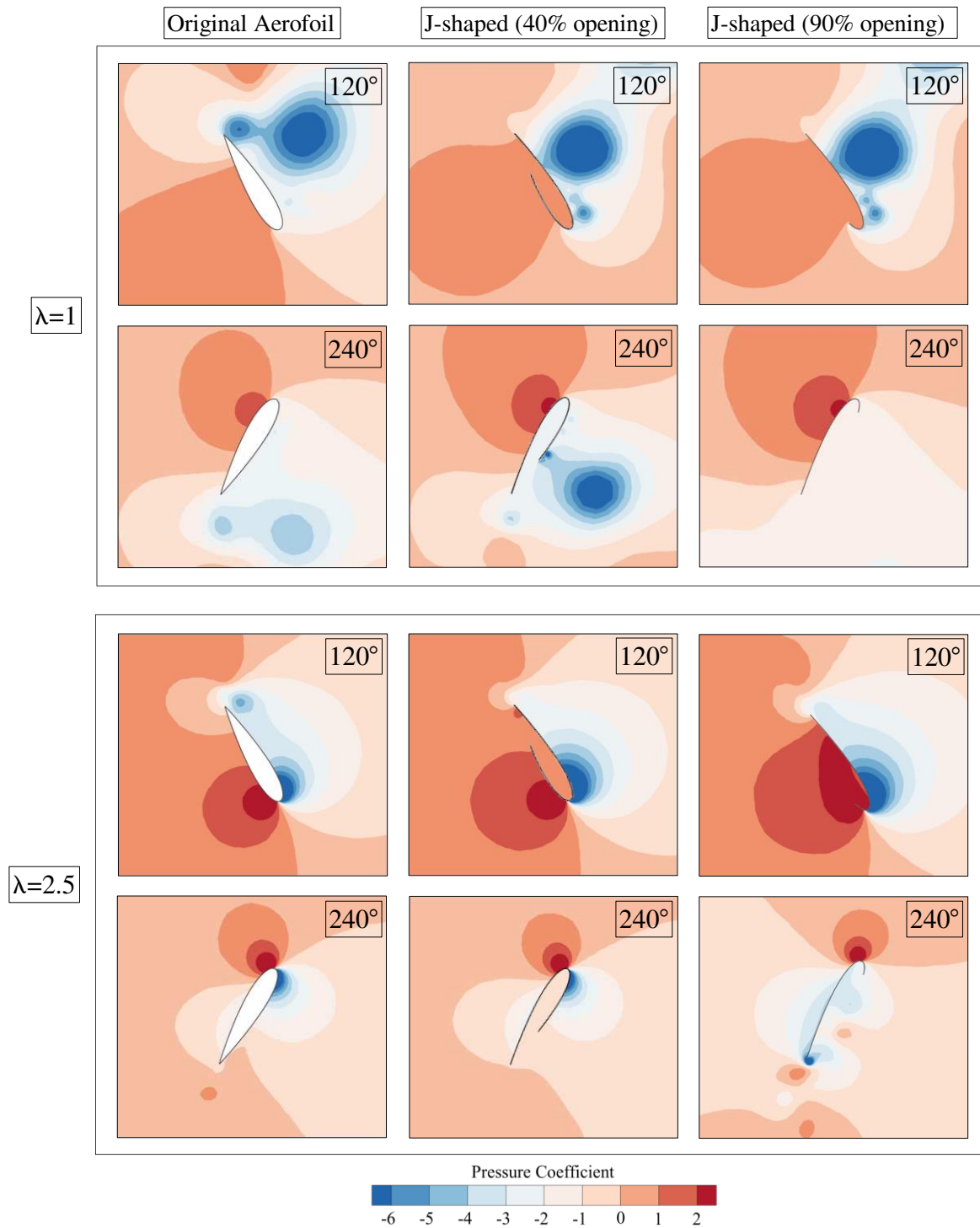

Fig. 17. The contours of pressure coefficient at the λ of 1 and 2.5 for original aerofoil and its J-shaped profiles with 40% and 90% opening ratios.

4.1.3. Contributions of lift and drag to turbine torque generation

Various λ values, such as 0.5, 1, 2.5, and 3.5, have been selected in order to study the contribution of the lift and drag to the torque generation of the turbine. Despite the fact that H-type VAWTs are called the lift-based turbine, the drag force may have a favourable impact on turbine torque output when λ is less than 1 [22]. The J-shaped aerofoil with different opening ratios is expected to contribute more positive drag to the torque generation compared to the original aerofoil profile. Therefore, in the present investigation, the original aerofoil profile (no cutting) and the J-shaped aerofoil with a 90% opening ratio have been selected due to the fact that the difference on the aerodynamic behaviour of these aerofoils is quite distinct.

Fig. 18 demonstrates the variation of the lift and drag force contributions to the turbine torque generation with the azimuthal angle for the original aerofoil profile and the J-shaped aerofoil with a 90% opening ratio at $\lambda = 0.5$ and $\lambda = 1$. At $\lambda = 0.5$, as can be observed in the figure, at the particular azimuthal angles of the entire revolution, especially between 120° and 240°, the lift force is not only main-driven force for the turbine, but also the drag force assists the turbine torque generation. In most of the azimuthal angles of the upstream part of the turbine, the positive lift contribution obtained from the J-shaped aerofoil with a 90% opening ratio is more significant than that of the original aerofoil profile, while the region of the positive drag contribution obtained from the J-shaped aerofoil with a 90% opening ratio is higher than that of the original aerofoil profile. This situation results in a much more positive net torque generation from the turbine with the J-shaped profile with a 90% opening ratio (see Fig. 12).

As the tip speed ratio approaches 1, the drag force's positive contribution reduces. However, at $\lambda = 1$, the J-shaped aerofoil with a 90% opening ratio still produce a higher positive lift force contribution at most of the azimuthal angles compared to the original aerofoil profile, while the negative drag force contributions appear to be similar for both aerofoils. That is the reason why the turbine with the J-shaped aerofoil with a 90% opening ratio generates a higher average turbine torque (see Fig. 12), which is beneficial to the turbine self-starting capability.
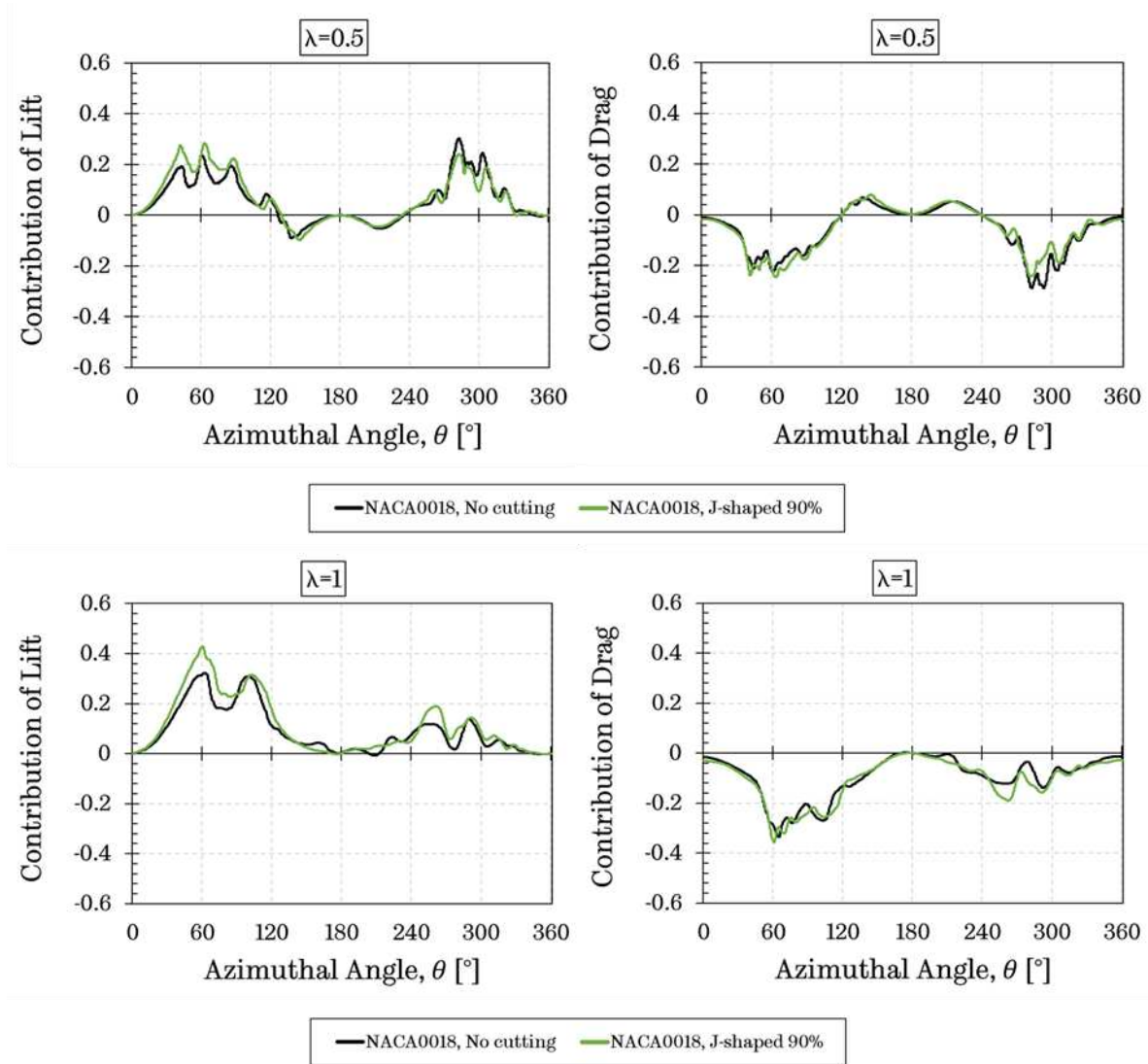
Fig. 18. Variation of the contribution of lift and drag to the torque generation with the azimuthal angle for the original aerofoil profile and the J-shaped aerofoil with a 90% opening ratio at λ = 0.5 and λ = 1.

The contributions of the lift and drag forces of the original aerofoil profile and the J-shaped aerofoil with a 90% opening ratio at λ = 2.5 and λ = 3.5 have been plotted in Fig. 19. As can be observed in the figure, the J-shaped profile with a 90% opening ratio provides a much greater positive lift contribution in the upstream part of the turbine, while the positive lift contribution of the original aerofoil profile is more significant in most of the azimuthal angles of the downstream part of the turbine at both tip speed ratios. In addition, regarding the negative drag contribution, the J-shaped aerofoil with a 90% opening ratio always produces a much greater negative drag contribution to the turbine torque generation at both λ values. This situation results in a lower overall performance of the turbine with the J-shaped aerofoil with a 90% opening ratio compared to the original aerofoil profile at high λ values.
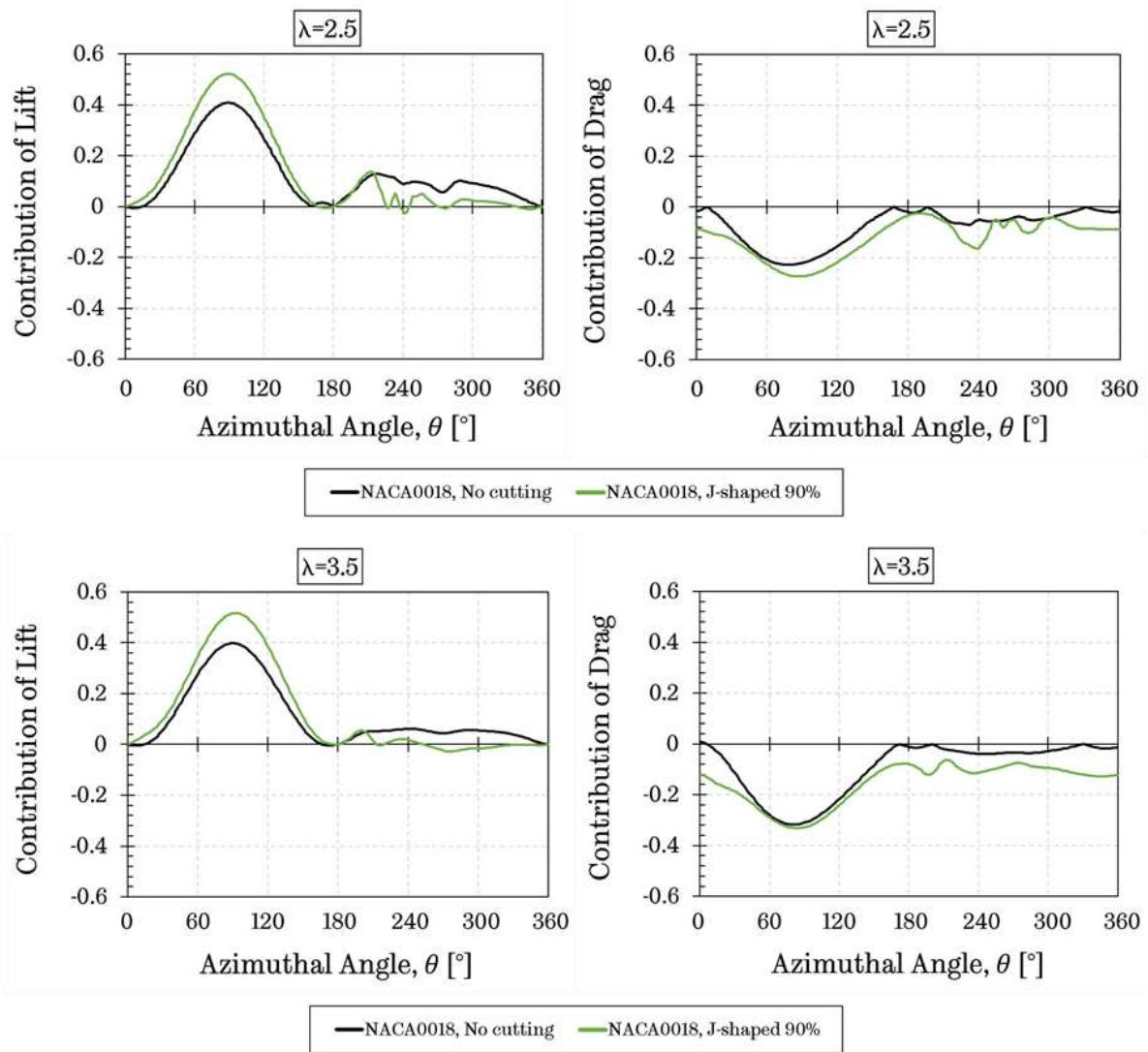
Fig. 19. Variation of the contribution of lift and drag to the torque generation with the azimuthal angle for the original aerofoil profile and the J-shaped aerofoil with a 90% opening ratio at λ = 2.5 and λ = 3.5.

4.2. Influence of the design parameters

4.2.1. Aerofoil profile

In the present section, four typical aerofoils generally used for H-type VAWT and their J-shaped profiles with different opening ratios have been investigated and compared in terms of the dynamic start-up behaviour. The aerofoil profiles investigated are as follows:

- NACA0012 and NACA0018 are the typical symmetrical NACA00xx series aerofoils and most widely used profiles for the H-type VAWT applications [55–57]. The purpose of choosing these two different profiles is to observe the effect of the aerofoil thickness with and without openings on the turbine self-starting behaviour.

- NACA2518 and NACA4518 are the cambered series of the NACA0018 aerofoil, which have the maximum camber of 2% and 4%, respectively, at 50% of the chord. As suggested by Kirke and Lazauskas [13] the cambered aerofoils may be able to demonstrate a better turbine performance, especially during the start-up period.

- Additionally, to fully examine the influence of the cambered aerofoils on the turbine self-starting, the reversed versions of these cambered aerofoils have been employed to the turbine blades considering the different opening ratios.

All investigations and comparisons have been performed by using the selected aerofoils with no cutting, 30%, 60%, and 90% opening ratios applied to the aerofoil's outer surface. Additionally, the concave side is the outer side of the NACA2518 and NACA4518, while that of the inner side for their reversed versions. The rotor radius and chord length have been chosen as $R = 0.375m$ and $c = 0.083m$, respectively, and the freestream wind speed was $V_\infty = 5m/s$.

Fig. 20 (a) illustrates the variation of the tip speed ratio with the time for the thinner aerofoil NACA0012 considering the different opening ratios. As can be seen in the figure, NACA0012 aerofoil with no cutting, 30%, and 60% opening ratios have given the worse self-starting performance; only the aerofoil with the highest opening ratio, $OR = 90\%$, tested is able to escape the plateau stage and reach the final steady-state condition. Furthermore, the NACA0018 J-shaped profile with the 30%, 60%, and 90% opening ratios demonstrate fully self-start characteristics. Although the start-up time decreases with the increase in the opening ratio, the final tip speed ratio in the steady-state condition decreases with the increase in the opening ratio (see Fig. 20 (b)). The findings reveal that the thicker aerofoil NACA0018 with even a shorter opening ratio, such as 30%, is able to self-start compared to the relatively thinner aerofoil NACA0012. It is also important to note that even though NACA0012 J-shaped aerofoil with a 90% opening ratio demonstrates a slower start-up characteristic compared to the NACA0018 aerofoil with a 90% opening ratio, its final tip speed ratio in the steady-state condition is much greater than that of the NACA0018 aerofoil. Nevertheless, the results indicate that the blade operating with the thicker aerofoil provides a much better self-starting characteristic with a wider range of the opening ratio at a tested freestream wind speed of $5m/s$.
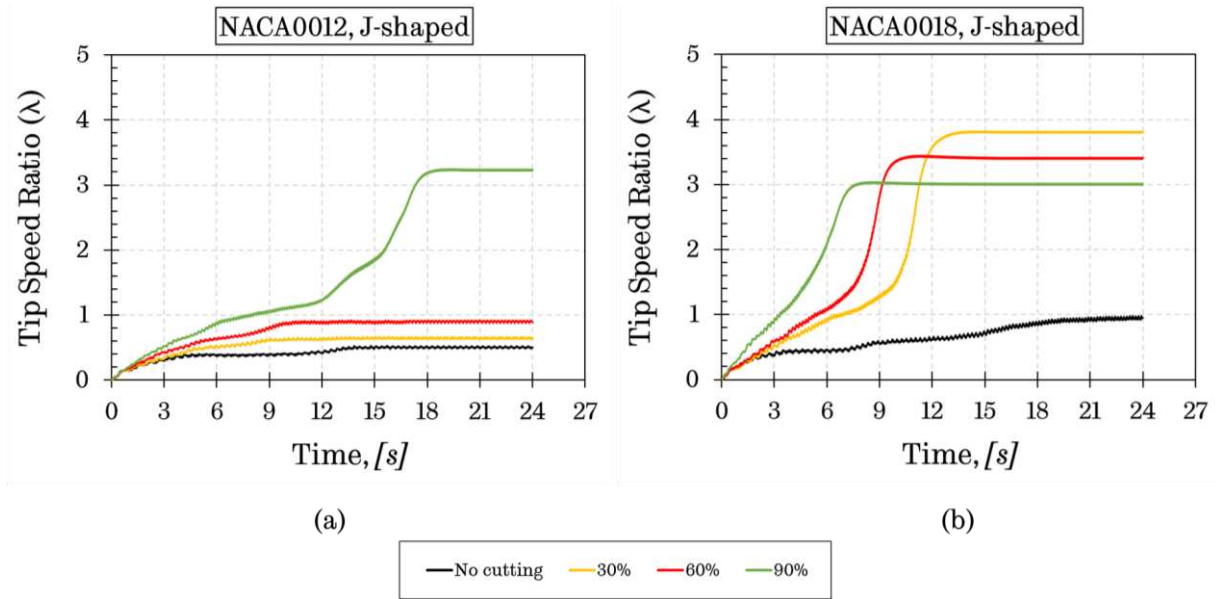
Fig. 20. Variation of the tip speed ratio with the time for NACA0012, NACA0018 and their J-shaped aerofoils for different opening ratios.

Fig. 21 illustrates the variation of the tip speed ratio with the time for the cambered aerofoil NACA2518 and its reversed version considering the different opening ratios. Fig. 21 (a) demonstrates that although the turbine with NACA2518 J-shaped profile with 60% and 90% opening ratios is able to self-start, the turbine with NACA2518 J-shaped profile with no cutting and 30% opening ratio fails to self-start. Furthermore, regarding its reversed version, the turbine with NACA2518 reversed aerofoil has also the self-starting capability even with a 30% opening ratio (see Fig. 21 (b)). With regards to the turbine's final tip speed ratio in the steady-state condition, the turbine with original NACA2518 and its reversed version having the opening ratio of 60% and 90% reach the steady-state condition at almost the same final tip speed ratios. However, although the start-up time of the turbine with NACA2518 reversed with a 90% opening ratio is much longer than that of the original NACA2518, the NACA2518 reversed aerofoil has a higher final tip speed ratio.
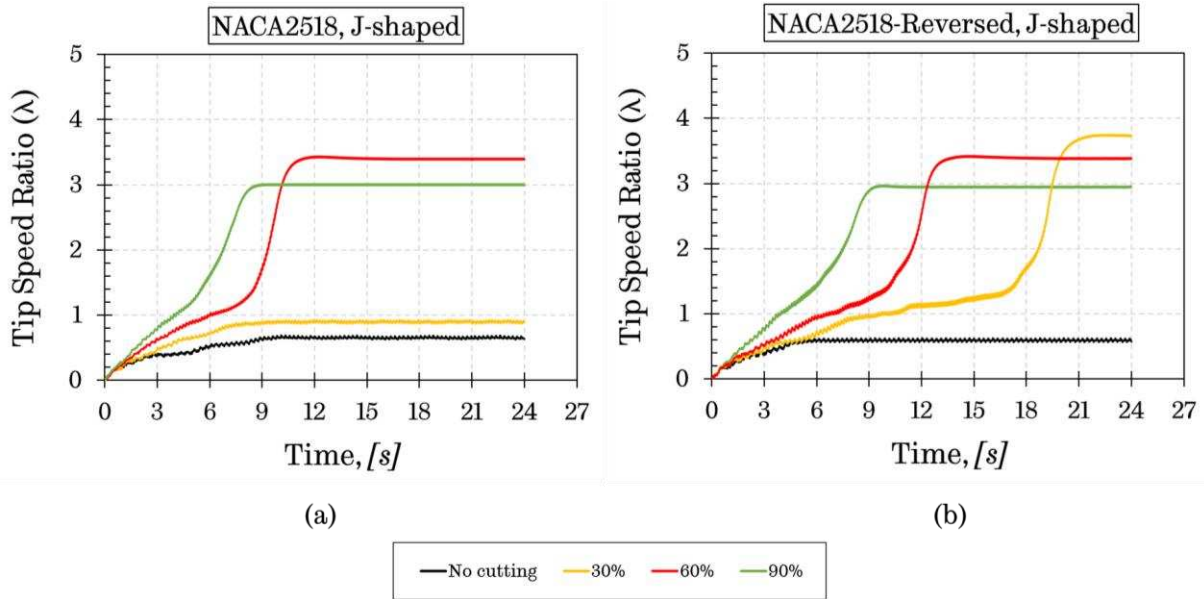
Fig. 21. Variation of the tip speed ratio with the time for NACA2518, NACA2518-reversed and their J-shaped aerofoils for different opening ratios.

Finally, the relatively high cambered aerofoil NACA4518 and its reversed version have been investigated and compared in Fig. 22. As seen in Fig. 22 (a), the use of the highly cambered aerofoil NACA4518 with the different values of the opening ratios, does not exhibit a remarkable self-starting characteristic, except the highest opening ratio, 90%, compared to the other opening ratios. On the other hand, its reversed version with 60% and 90% opening ratios are still able to escape the plateau stage and reach to their steady-state conditions (see Fig. 22 (b)).
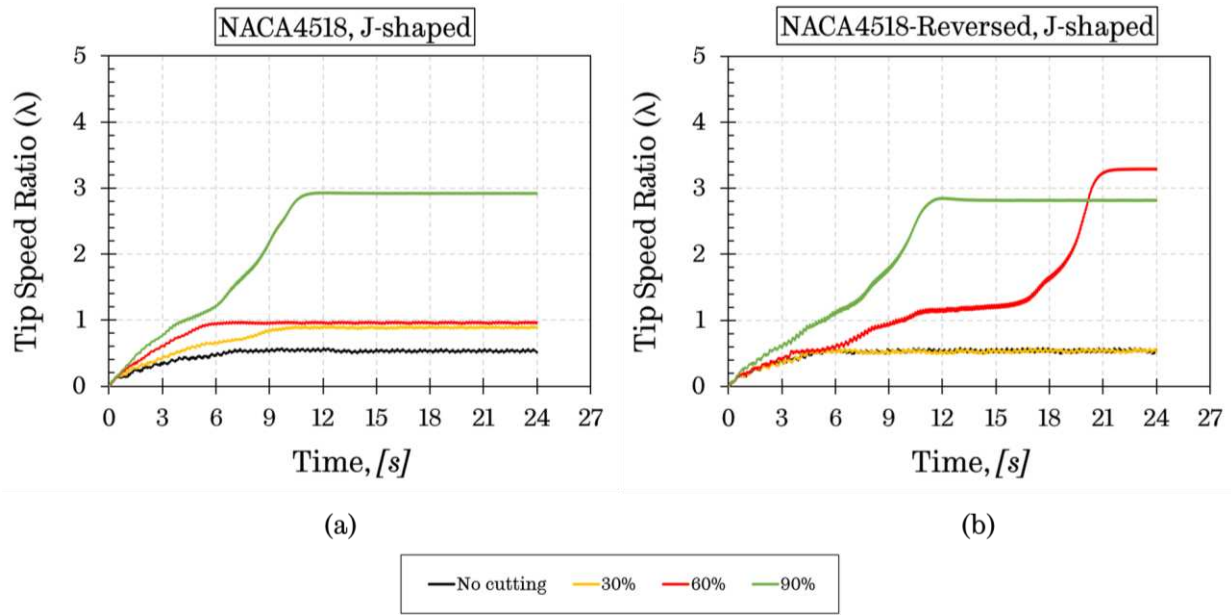
Fig. 22. Variation of the tip speed ratio with the time for NACA4518, NACA4518-reversed and their J-shaped aerofoils for different opening ratios.
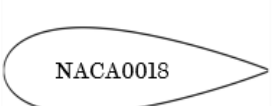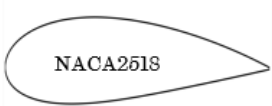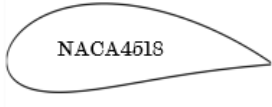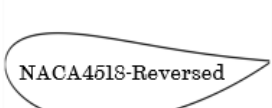
In conclusion, the results obtained from the analyses of the effect of the aerofoil profile with and without an opening on the turbine dynamic start-up behaviour are summarised in Table 2. As can be observed in the table, NACA0012, NACA4518 and their J-shaped profiles do not appear to bring a significant benefit compared to the NACA0018 aerofoil and its J-shaped profiles. The results of this investigation also show that the turbine with all the aerofoil profiles investigated with a 90% opening ratio can escape the plateau stage and reach its steady-state condition; however, the original aerofoils, which have no cutting on the surface, cannot self-start at the tested upstream wind speed of $5 m/s$.

The findings of the current study also suggest that even though the thinner aerofoil NACA0012 can exhibit a higher final tip speed ratio at the steady-state condition when a 90% opening ratio is applied, the thicker aerofoil NACA0018 provides a better self-starting characteristic with a wider range of the opening ratio compared to the thinner aerofoil NACA0012. These results are consistent with those of the other studies and suggest that the thicker aerofoils are able to enhance the turbine performance, in particular at the low λ values, which may lead to improve the self-starting capability [13,55,58].

The most obvious finding to emerge from this study was that the reversed versions of the cambered aerofoils investigated demonstrate a better self-starting capability compared to their original profiles. However, in comparison with the thicker aerofoil NACA0018 and its J-shaped profiles,

the original and reversed cambered aerofoils do not show any improvement on the self-starting capability when the start-up time and final tip speed ratio are taken into account.

Table 2. The comparison of the self-starting capabilities of the aerofoils investigated in terms of the self-starting time and final tip speed ratio.

	Self-starting capability				Self-starting time (s)				Final λ			
	0%	30%	60%	90%	0%	30%	60%	90%	0%	30%	60%	90%
NACA0012	NO	NO	NO	YES	—	—	—	19.7	—	—	—	3.23
NACA0018	NO	YES	YES	YES	—	15.2	12.2	9.2	—	3.81	3.41	2.99
NACA2518	NO	NO	YES	YES	—	—	14.6	10.4	—	—	3.38	2.99
NACA2518-Reversed	NO	YES	YES	YES	—	23.4	16.02	12.03	—	3.73	3.37	2.95
NACA4518	NO	NO	NO	YES	—	—	—	12.55	—	—	—	2.91
NACA4518-Reversed	NO	NO	YES	YES	—	—	22.9	13.78	—	—	2.28	2.81

4.2.2. Pitch angle

The active pitch control mechanism can enable the turbine blades to produce the optimum torque at the low tip speed ratio regions, which results in a better turbine power output and self-starting ability [59]. However, due to the fact that the small-scale H-type VAWT has been considered in the present study, the active pitch control mechanism is not taken into account due to its complexity

and it being economically not viable. Instead of the active pitch control, another alternative way to change the aerodynamics of the blades during a complete revolution is to utilize the fixed pitch angle and its impact on the turbine dynamic start-up behaviour will be investigated numerically.

The numerical investigations have been performed at the seven values of the fixed pitch angles, which are -8°, -4°, -2°, 0° (no pitch), 2°, 4° and 8°, and the definition of the pitch angle for the current investigation is shown in Fig. 23. The aerofoil profiles used in the present study are the conventional aerofoil NACA0018 and its J-shaped profiles with 30%, 60%, and 90% opening ratios with a rotor radius $R = 0.375m$ and blade chord length $c = 0.083m$. The upstream free wind speed was $V_\infty = 5m/s$.
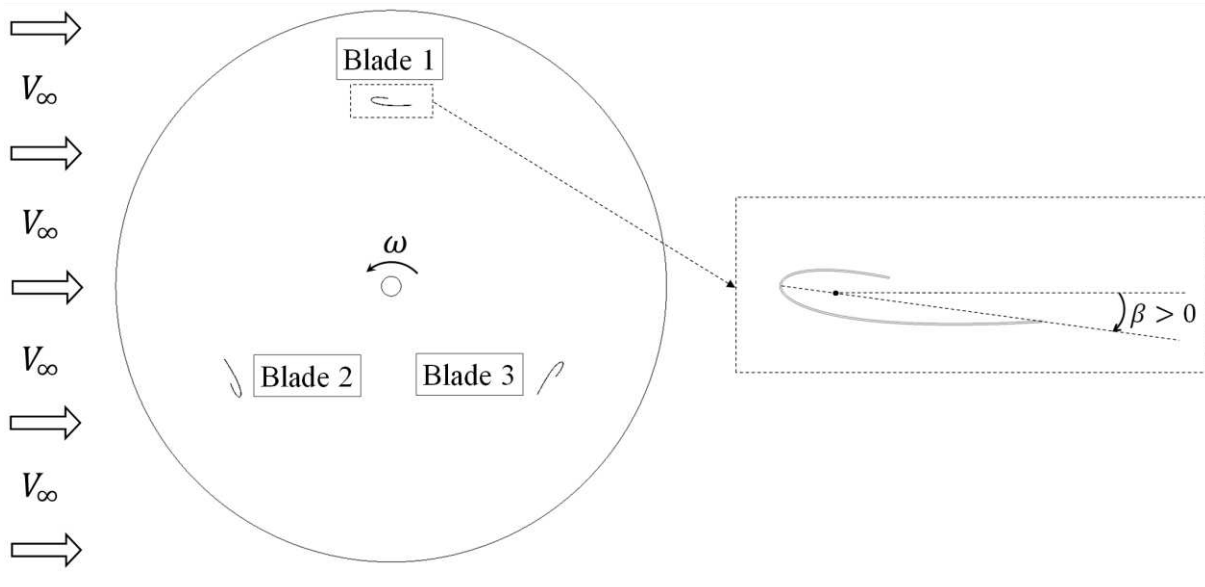
Fig. 23. The definition of the pitch angle used in the current study.

Fig. 24 presents the variation of the tip speed ratio with the time for the different values of the fixed pitch angles considering the conventional aerofoil NACA0018 and its J-shaped profiles with 30%, 60%, and 90% opening ratios. Using the conventional aerofoil NACA0018, Fig. 24 (a) shows the influence of varied fixed pitch angle values on turbine self-starting performance. As it can be seen in the figure that the conventional aerofoil with all the fixed pitch angles investigated cannot assist the turbine to self-start and the value of the final tip speed ratio reduces with the most negative value of the pitch angle. At the opening ratio, OR = 30%, (see Fig. 24 (b)), the turbine with the blade pitch angles of $\beta = 2°$ and $\beta = 4°$ improve the turbine self-starting performance in terms of the turbine start-up time compared to pitch angle of $\beta = 0°$. However, the results reveal that a

positively further increase in the pitch angle does not help the turbine to self-start if the 30% opening ratio is employed. Moreover, regarding the negative pitch angles, the self-starting behaviour gets worse at all the negative pitch angles investigated. Concerning the J-shaped profile with a 60% opening ratio (see Fig. 24 (c)), the positive pitched blades are able to enhance the turbine self-starting capability compared to the negative pitched blades. In addition to this, although the turbine with the blade pitch angles of $\beta = 2°$ and $\beta = 4°$ reaches the steady-state condition at almost the same final tip speed ratio as the blade without a pitch angle, the blade with the blade pitch angles of $\beta = 4°$ shows a faster start-up time. However, the turbine with the most positive pitch angle ($\beta = 8°$) significantly degrades the turbine final tip speed ratio. At the opening ratio, $OR = 90\%$, the advantages and disadvantages of the pitch angle become much more obvious. As can be observed in Fig. 24 (d), the turbine self-starting time decreases with the changing the blade pitch angle from $\beta = 2°$ to $\beta = 8°$. Unlike the effect of the negative pitched angles on the turbine self-starting behaviour with 30% and 60% opening ratios, by employing a slightly negative pitched blade of $\beta = -2°$ also shows an improved self-starting performance in terms of the final tip speed ratio at the steady-state condition. However, with this slightly negative pitch angle, the turbine self-starts much later, and a much slower turbine acceleration can be observed during the plateau stage.
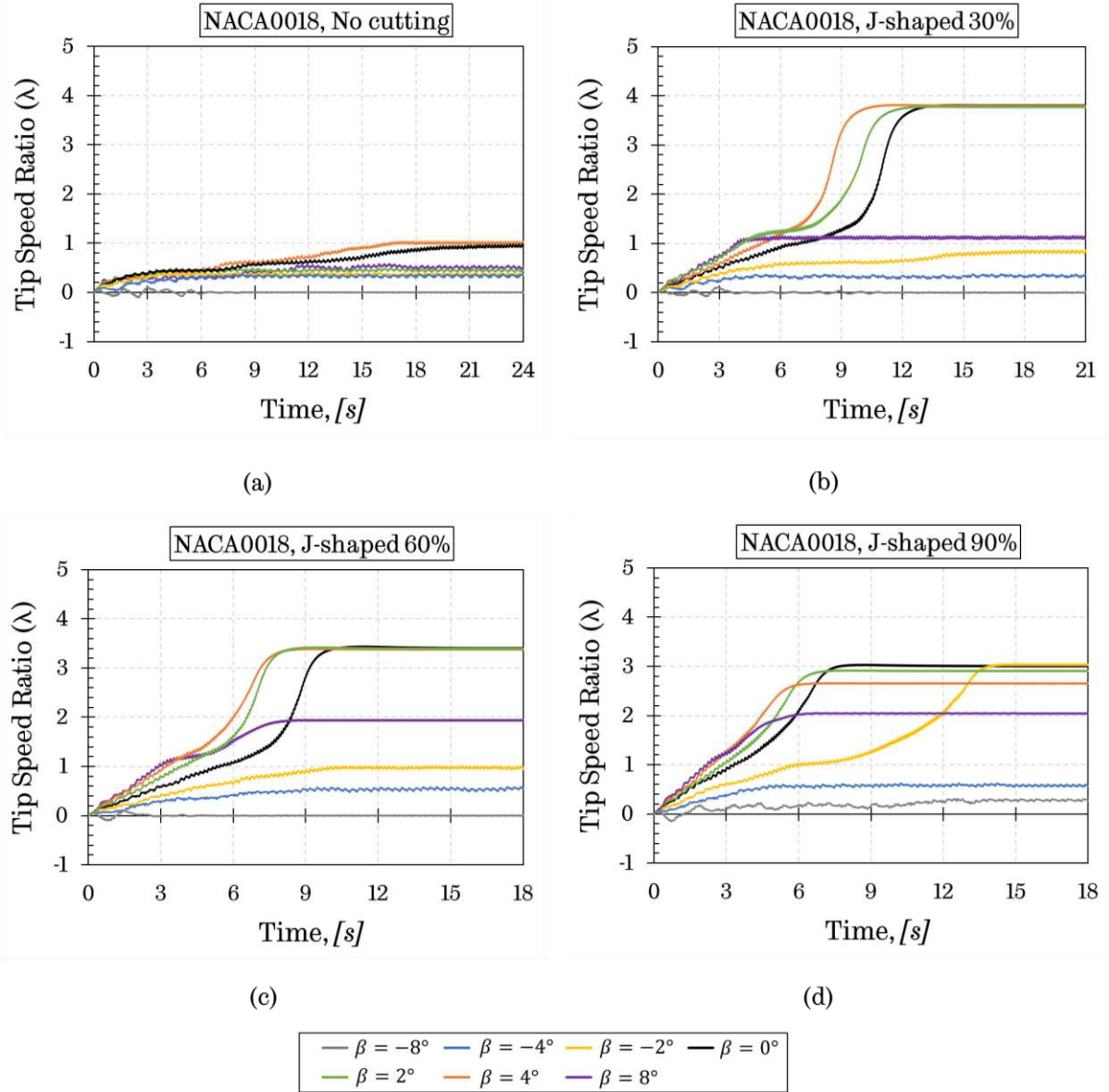
Fig. 24. Variation of the tip speed ratio with the time for different values of the fixed-pitch angles considering the conventional aerofoil NACA0018 and its J-shaped profiles with 30%, 60%, and 90% opening ratios.

A further study has been conducted by investigating at the instantaneous torque coefficients for the different pitch angles using the J-shaped aerofoil with 90% and 60% opening ratios at the tip speed ratio of $\lambda = 1.6$ and $\lambda = 3.38$, respectively. For the J-shaped aerofoil with a 90% opening ratio at $\lambda = 1.6$ (Fig. 25), where the blade still experiences the dynamic stall, the peak torque coefficients for $\beta = 8°$, $\beta = 4°$, $\beta = 2°$, $\beta = 0°$, and $\beta = -2°$ have been obtained at $\theta = 89.4°$, $\theta = 85.8°$, $\theta = 82.4°$, $\theta = 78°$, and $\theta = 75.7°$, respectively. The positive pitch angles successfully delay the stall and enable the blade to produce more torque for a greater portion of the azimuthal angle. However, the blade performance in the downstream part of the turbine significantly decreases by

the large positive pitch angle. The pitch angle of $\beta = 8°$ produces a negative torque in the azimuthal angles between $\theta = 200°$ and $\theta = 360°$, which offsets the positive contribution of the blade in the upstream part of the turbine and may lead to lower torque generation at all the start-up stages. With regards to the negative pitch angle $\beta = -2°$, the stall occurs earlier than $\beta = 0°$ at $\theta = 75.7°$ as shown in Fig. 25. Although the negative pitch angle yields better blade performance in the downstream part of the turbine, the much deteriorated torque generation has been obtained in the upstream part, which may result in a much slower turbine acceleration during the plateau stage (see Fig. 24 (d)).

Fig. 25. Variation of the instantaneous torque coefficient with the azimuthal angle for different pitch angles using the J-shaped aerofoil with 90% opening ratio at the tip speed ratio of $\lambda = 1.6$.

Furthermore, Fig. 26 illustrates the instantaneous torque coefficient for the J-shaped aerofoil with a 60% opening ratio at $\lambda = 3.38$, where the blade no longer experiences stall. Compared to $\beta = 0°$, while the positive pitch angle, such as $\beta = 2°$ or $\beta = 4°$, enhances the torque generation in the downstream part of the turbine, the overall torque coefficients are almost the same due to the reduced torque efficiency in the upstream part of the turbine. Therefore, the turbine with $\beta = 4°, 2°,$ and $0°$ reaches the steady-state condition at almost the same final tip speed ratio (see Fig. 24 (c)).
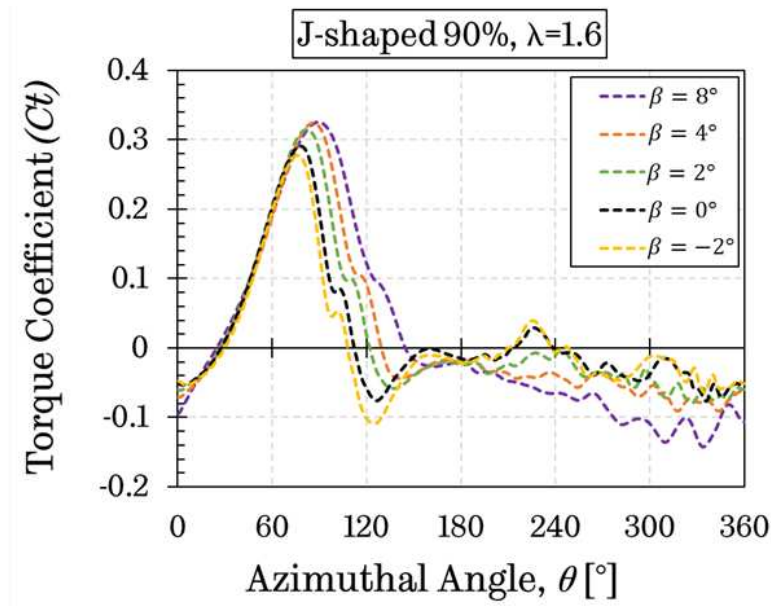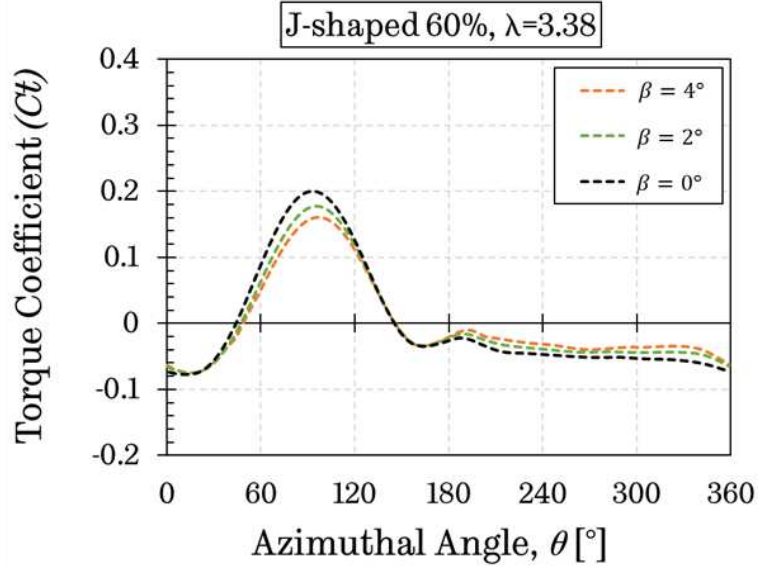
Fig. 26. Variation of the instantaneous torque coefficient with the azimuthal angle for different pitch angles using the J-shaped aerofoil with 60% opening ratio at the tip speed ratio of $\lambda = 3.38$.

Since the majority portion of the torque is produced by the blade in the upstream part of the turbine, a positive pitched blade can delay the blade stall and assist the blade generates more torque over a greater portion of the upstream part of the turbine at the low λ values. This delayed stall is responsible for the improved turbine performance measured at the low λ values, which might be beneficial for the turbine to enhance the self-starting capability. However, the highly negative torque produced in the downstream part of the turbine may provide a negative contribution to the overall torque generation, which is not desirable for the turbine self-starting (e.g. $\beta = 8°$). With the increase in the tip speed ratio, the blade angle of attack variation is significantly reduced and above a critical tip speed ratio, the blade no longer experiences stall during the complete turbine revolution. In terms of the relatively high tip speed ratios, a positive pitch angle decreases the blade angle of attack in the upstream region resulting in less torque produced. On the contrary, this positive pitch angle also increases the blade angle of attack in the downstream part of the turbine; therefore, the blade is able to capture the high possibility of the torque generated compared to the blade with no pitch.

In a conclusion, the findings in this section reveal that the pitch angle has a different effect depending on the J-shaped aerofoil with the different value of the opening ratios. Although the pitched J-shaped aerofoil has mixed effects on the turbine performance in different tip speed ratios, the J-shaped turbine with a slightly positive pitched blade ($\beta = 2°$) clearly illustrates a better start-up time in all cases investigated and a similar final tip speed ratio value at the steady-state condition compared to the $\beta = 0°$. On the contrary, the negative pitch angles do not bring any benefits with

36

the J-shaped aerofoil, except the turbine with 90% opening ratio J-shaped aerofoil with a slightly negative pitch angle ($\beta = -2°$). In addition, a too large negative pitch angle, such as $\beta = -4°$ and $\beta = -8°$, prevents the turbine from self-starting in all the cases investigated.

5. Conclusion

In the present study, a three bladed H-type VAWT with original aerofoils and their J-shaped profiles having a different number of the opening ratios have been analysed to evaluate the impact of an aerofoil with and without openings on the turbine performance. This study focuses on the self-starting performance and overall efficiency of the turbine with J-shaped profiles considering the dynamic start-up model, which has not been used in the previous studies. The information provided from the present study can be applied to a small-scale VAWT design having the J-shaped aerofoil in order to enhance the self-starting ability and also reduce performance loss occurred at the high turbine speed regimes.

According to the numerical results obtained in the current study, several important conclusions and recommendations can be drawn:

- The investigations presented here strongly recommended that although the torque coefficient versus tip speed ratio curve is able to provide an indication of the self-starting performance according to the torque generation at the low λ values, a further analysis, namely the turbine dynamic start-up curve, is required in order to fully understand the self-starting process of the turbine having the J-shaped aerofoils.

- The turbine with the J-shaped aerofoil having the openings located at the inner surface does not appear to bring any benefit and makes the choice of the inner profiles unreasonable compared with the outer surface.

- The effect of the J-shaped aerofoil with different opening ratios, which are located at the outer surface, may differ depending on the tip speed ratio. For instance, the largest opening ratio, which is the 90% in the present study, has a better performance at the low tip speed ratios, while the original aerofoil profile (no cutting) has the better performance at the higher tip speed ratio. Therefore, the selection of the optimum opening ratio completely depends on the purpose of the turbine. If a good self-starting performance is required, then the largest opening ratio should be preferred but there is a larger penalty at the higher tip speed ratios, and this must be considered.

- The turbine with the original aerofoil profile and the J-shaped aerofoil with a 10% opening ratio is not able to accelerate and escape the plateau stage due to the negative torque generation at the critical range of the tip speed ratio (e.g., $0.5 < \lambda < 1.5$).

- Among the six different aerofoil profiles that have been investigated, the worst self-starting performance has been obtained by the thinner aerofoil NACA0012 and the highly cambered aerofoil NACA4518. However, the thicker aerofoil NACA0018 and cambered NACA218-reversed have been demonstrated to be a good choice for the H-type VAWT from the point of view of the self-starting characteristics. In addition, the reversed version of the cambered aerofoils investigated demonstrate a better self-starting capability compared to their original profiles.

- The turbine with the J-shaped aerofoil having a slightly positive pitch angle ($\beta = 2°$) clearly illustrates a better start-up capability in all cases investigated and a similar final tip speed ratio value at the steady-state condition compared to the $\beta = 0°$. However, the negative pitch angles do not bring any benefits to the H-type VAWT with the J-shaped aerofoil.

Nomenclature

C_d	Drag coefficient [-]
C_l	Lift coefficient [-]
C_t	Torque coefficient [-]
F_d	Drag force [N]
F_l	Lift force [N]
R	Radius of the turbine [m]
T_{res}	Resistive torque [N.m]
T_w	Wind torque [N.m]
OR	Opening ratio over aerofoil surface [-]
V_∞	Free stream wind velocity [m/s]
α	Angle of attack [°]
β	Blade pitch angle [°]
θ	Azimuthal angle [°]
λ	Tip speed ratio [-]
I	Turbine moment of inertia [kgm²]
ω	Rotational speed of the turbine [rad/s]

Appendix

The following is the UDF code that includes the physical properties such as turbine mass, moment of inertia, and resistive torque (if available) has been employed in the 2D CFD simulations to calculate the turbine rotational speed. The moment of the inertia of the turbine has been calculated depending on the per unit span.

```c
#include "udf.h"

DEFINE_SDOF_PROPERTIES(rotor, prop, dt, time, dtime)
{
   prop[SDOF_MASS]        = 0.213;
   prop[SDOF_IXX]         = 0.03;
   prop[SDOF_IYY]         = 0.03;
   prop[SDOF_IZZ]         = 0.03;

   prop[SDOF_ZERO_TRANS_X] = TRUE;
   prop[SDOF_ZERO_TRANS_Y] = TRUE;
   prop[SDOF_ZERO_TRANS_Z] = TRUE;

   prop[SDOF_ZERO_ROT_X] = TRUE;
   prop[SDOF_ZERO_ROT_Y] = TRUE;
   prop[SDOF_ZERO_ROT_Z] = FALSE;

   prop[SDOF_LOAD_M_X]    = 0;
   prop[SDOF_LOAD_M_Y]    = 0;
   prop[SDOF_LOAD_M_Z]    = -0.002*DT_OMEGA_CG(dt)[2];  /* variable
resistive torque */

   printf ("\n Blade updated 6DOF properties");
}
```

References

[1]   Zhao Z, Wang D, Wang T, Shen W, Liu H, Chen M. A review: Approaches for aerodynamic performance improvement of lift-type vertical axis wind turbine. Sustain Energy Technol Assessments 2022;49:101789. https://doi.org/10.1016/j.seta.2021.101789.

[2]   Hand B, Cashman A. A review on the historical development of the lift-type vertical axis wind turbine: From onshore to offshore floating application. Sustain Energy Technol Assessments 2020;38. https://doi.org/10.1016/j.seta.2020.100646.

[3]   Kaya MN, Kose F, Ingham D, Ma L, Pourkashanian M. Aerodynamic performance of a horizontal axis wind turbine with forward and backward swept blades. J Wind Eng Ind Aerodyn 2018;176:166–73. https://doi.org/10.1016/j.jweia.2018.03.023.

[4]   Rezaeiha A, Montazeri H, Blocken B. Characterization of aerodynamic performance of vertical axis wind turbines: Impact of operational parameters. Energy Convers Manag 2018;169:45–77. https://doi.org/10.1016/j.enconman.2018.05.042.

[5]   Du L. Numerical and Experimental Investigations of Darrieus Wind Turbine Start-up and

Operation. Durham Univ , PhD Thesis 2016.

[6]   Worasinchai S. Small Wind Turbine Starting Behaviour. Durham University, PhD Thesis, 2012.

[7]   Baker JR. Features to aid or enable self starting of fixed pitch low solidity vertical axis wind turbines. J Wind Eng Ind Aerodyn 1983;15:369–80. https://doi.org/10.1016/0167-6105(83)90206-4.

[8]   B. K. Kirke. Evaluation of Self-Starting Vertical Axis Wind Turbines for Stand-Alone Appllications. Griffith University, Australia, PhD Thesis, 1998.

[9]   Ebert PR, Wood DH. Observations of the starting behavior of a small horizontal- axis wind turbine. Renew Energy 1997;12:245–57.

[10]   Lunt PAV. An aerodynamic model for a vertical-axis wind turbine. MEng project report,School of Engineering, University of Durham, UK, 2005.

[11]   Celik Y. Aerodynamics and Self-Starting of Vertical Axis Wind Turbines with J-Shaped Aerofoils. Univ Sheffield, PhD Thesis 2021.

[12]   Wang Y, Sun X, Dong X, Zhu B, Huang D, Zheng Z. Numerical investigation on aerodynamic performance of a novel vertical axis wind turbine with adaptive blades. Energy Convers Manag 2016;108:275–86. https://doi.org/10.1016/j.enconman.2015.11.003.

[13]   Kirke, B.K. and Lazauskas L. Enhancing the performance of vertical axis wind turbine using a simple variable pitch system. Wind Eng 1991;187–195.

[14]   Healy JV. The influence of blade camber on the output of vertical-axis wind turbines. Wind Eng 1978:146–55.

[15]   Bianchini A, Balduzzi F, Rainbird JM, Peiró J, Graham JMR, Ferrara G, et al. On the influence of virtual camber effect on airfoil polars for use in simulations of Darrieus wind turbines. Energy Convers Manag 2015;106:373–84. https://doi.org/10.1016/j.enconman.2015.09.053.

[16]   Islam M, Ting DS-K, Fartaj A. Desirable airfoil features for smaller-capacity straight-bladed VAWT. Wind Eng 2007;31:165–96. https://doi.org/10.1260/030952407781998800.

[17]   Chen J, Yang H, Yang M, Xu H. The effect of the opening ratio and location on the performance of a novel vertical axis Darrieus turbine. Energy 2015;89:819–34.

https://doi.org/10.1016/j.energy.2015.05.136.

[18] Zamani M, Maghrebi MJ, Varedi SR. Starting torque improvement using J-shaped straight-bladed Darrieus vertical axis wind turbine by means of numerical simulation. Renew Energy 2016;95:109–26. https://doi.org/10.1016/j.renene.2016.03.069.

[19] Mohamed MH. Criticism study of J-Shaped darrieus wind turbine: Performance evaluation and noise generation assessment. Energy 2019;177:367–85. https://doi.org/10.1016/j.energy.2019.04.102.

[20] Rainbird J. The aerodynamic development of a vertical axis wind turbine. MEng Proj ReporSchool Eng Univ Durham, UK 2007.

[21] Zhu J, Huang H, Shen H. Self-starting aerodynamics analysis of vertical axis wind turbine. Adv Mech Eng 2015;7:1–12. https://doi.org/10.1177/1687814015620968.

[22] Celik Y, Ma L, Ingham D, Pourkashanian M. Journal of Wind Engineering & Industrial Aerodynamics Aerodynamic investigation of the start-up process of H-type vertical axis wind turbines using CFD. J Wind Eng Ind Aerodyn 2020;204. https://doi.org/10.1016/j.jweia.2020.104252.

[23] Sun X, Zhu J, Hanif A, Li Z, Sun G. Effects of blade shape and its corresponding moment of inertia on self-starting and power extraction performance of the novel bowl-shaped floating straight-bladed vertical axis wind turbine. Sustain Energy Technol Assessments 2020;38:100648. https://doi.org/10.1016/j.seta.2020.100648.

[24] Elsakka MM, Ingham DB, Ma L, Pourkashanian M. Comparison of the Computational Fluid Dynamics Predictions of Vertical Axis Wind Turbine Performance Against Detailed Pressure Measurements. Int J Renew Energy Res 2021;11:276–93.

[25] Rezaeiha A, Montazeri H, Blocken B. Towards accurate CFD simulations of vertical axis wind turbines at different tip speed ratios and solidities: Guidelines for azimuthal increment, domain size and convergence. Energy Convers Manag 2018;156:301–16. https://doi.org/10.1016/j.enconman.2017.11.026.

[26] Rezaeiha A, Kalkman I, Montazeri H, Blocken B. Effect of the shaft on the aerodynamic performance of urban vertical axis wind turbines. Energy Convers Manag 2017;149:616–30. https://doi.org/10.1016/j.enconman.2017.07.055.

[27] Elsakka MM, Ingham DB, Ma L, Pourkashanian M. CFD analysis of the angle of attack for a vertical axis wind turbine blade. Energy Convers Manag 2019;182:154–65.

https://doi.org/10.1016/j.enconman.2018.12.054.

[28] Kaya MN, Kök AR, Kurt H. Comparison of aerodynamic performances of various airfoils from different airfoil families using CFD. Wind Struct An Int J 2021;32:239–48. https://doi.org/10.12989/was.2021.32.3.239.

[29] Syawitri TP, Yao Y, Yao J, Chandra B. Geometry optimisation of vertical axis wind turbine with Gurney flap for performance enhancement at low , medium and high ranges of tip speed ratios. Sustain Energy Technol Assessments 2022;49:101779. https://doi.org/10.1016/j.seta.2021.101779.

[30] Kaya MN, Köse F, Uzol O, Ingham D, Ma L, Pourkashanian M. Aerodynamic Optimization of a Swept Horizontal Axis Wind Turbine Blade. J Energy Resour Technol 2021;143. https://doi.org/10.1115/1.4051469.

[31] Mazarbhuiya HMSM, Biswas A, Sharma KK. Blade thickness effect on the aerodynamic performance of an asymmetric NACA six series blade vertical axis wind turbine in low wind speed. Int J Green Energy 2020;17:171–9. https://doi.org/10.1080/15435075.2020.1712214.

[32] Wekesa DW, Wang C, Wei Y, Zhu W. Experimental and numerical study of turbulence effect on aerodynamic performance of a small-scale vertical axis wind turbine. J Wind Eng Ind Aerodyn 2016;157:1–14. https://doi.org/10.1016/j.jweia.2016.07.018.

[33] Song C, Zheng Y, Zhao Z, Zhang Y, Li C, Jiang H. Investigation of meshing strategies and turbulence models of computational fluid dynamics simulations of vertical axis wind turbines. J Renew Sustain Energy 2015;7. https://doi.org/10.1063/1.4921578.

[34] Rezaeiha A, Montazeri H, Blocken B. On the accuracy of turbulence models for CFD simulations of vertical axis wind turbines. Energy 2019;180:838–57. https://doi.org/10.1016/j.energy.2019.05.053.

[35] Greenblatt D, Schulman M, Ben-harav A. Vertical axis wind turbine performance enhancement using plasma actuators. Renew Energy 2012;37:345–54. https://doi.org/10.1016/j.renene.2011.06.040.

[36] Batista NC, Melício R, Mendes VMF, Calderón M, Ramiro A. On a self-start Darrieus wind turbine: Blade design and field tests. Renew Sustain Energy Rev 2015;52:508–22. https://doi.org/10.1016/j.rser.2015.07.147.

[37] Wang S, Ingham DB, Ma L, Pourkashanian M, Tao Z. Numerical investigations on

dynamic stall of low Reynolds number flow around oscillating airfoils. Comput Fluids 2010;39:1529–41. https://doi.org/10.1016/j.compfluid.2010.05.004.

[38]   Lee J, Zhao F. GWEC Global Wind Report. Wind Energy Technol 2020:78.

[39]   Kinzel M, Mulligan Q, Dabiri JO. Energy exchange in an array of vertical-axis wind turbines. J Turbul 2012;13:1–13. https://doi.org/10.1080/14685248.2012.712698.

[40]   McCroskey, W. J., Carr, L. W., & McAlister KW. Dynamic stall experiments on oscillating airfoils. Aiaa J 1976:57–63.

[41]   Mohamed MH, Dessoky A, Alqurashi F. Blade shape effect on the behavior of the H-rotor Darrieus wind turbine: Performance investigation and force analysis. Energy 2019;179:1217–34. https://doi.org/10.1016/j.energy.2019.05.069.

[42]   Amano R, Sunden B. Aerodynamics of wind turbines: emerging topics. WIT Press; 2014.

[43]   Hand B, Kelly G, Cashman A. Numerical simulation of a vertical axis wind turbine airfoil experiencing dynamic stall at high Reynolds numbers. Comput Fluids 2017;149:12–30. https://doi.org/10.1016/j.compfluid.2017.02.021.

[44]   Nobile R, Vahdati M, Barlow JF, Mewburn-Crook A. Unsteady flow simulation of a vertical axis augmented wind turbine: A two-dimensional study. J Wind Eng Ind Aerodyn 2014;125:168–79. https://doi.org/10.1016/j.jweia.2013.12.005.

[45]   Posa A. Influence of Tip Speed Ratio on wake features of a Vertical Axis Wind Turbine. J Wind Eng Ind Aerodyn 2020;197:104076. https://doi.org/10.1016/j.jweia.2019.104076.

[46]   Rezaeiha A, Kalkman I, Blocken B. CFD simulation of a vertical axis wind turbine operating at a moderate tip speed ratio: Guidelines for minimum domain size and azimuthal increment. Renew Energy 2017;107:373–85. https://doi.org/10.1016/j.renene.2017.02.006.

[47]   Almohammadi KM, Ingham DB, Ma L, Pourkashan M. Computational fluid dynamics (CFD) mesh independency techniques for a straight blade vertical axis wind turbine. Energy 2013;58:483–93. https://doi.org/10.1016/j.energy.2013.06.012.

[48]   ANSYS. ANSYS Fluent User's Guide Release 15.0. Canonsburg: ANSYS Inc.: 2013.

[49]   Kortleven M. Simulation Verification and Optimization of a Vertical Axis Wind Turbine using CFD 2016.

[50] Naseem A, Uddin E, Ali Z, Aslam J, Shah SR, Sajid M, et al. Effect of vortices on power output of vertical axis wind turbine (VAWT). Sustain Energy Technol Assessments 2020;37:100586. https://doi.org/10.1016/j.seta.2019.100586.

[51] Untaroiu A, Wood HG, Allaire PE, Ribando RJ. Investigation of Self-Starting Capability of Vertical Axis Wind Turbines Using a Computational Fluid Dynamics Approach. J Sol Energy Eng 2011;133:041010. https://doi.org/10.1115/1.4004705.

[52] Torabi M, Zal E, Mustapha F, Wiriadidjaja S. Study on start-up characteristics of H-Darrieus vertical axis wind turbines comprising NACA 4-digit series blade airfoils. Energy 2016;112:528–37. https://doi.org/10.1016/j.energy.2016.06.059.

[53] Almohammadi K, Ingham D, Ma L, Pourkashanian M. CFD sensitivity analysis of a straight-blade vertical axis wind turbine. Wind Eng 2012;36:571–88. https://doi.org/10.1260/0309-524X.36.5.571.

[54] Daróczy L, Janiga G, Petrasch K, Webner M, Thévenin D. Comparative analysis of turbulence models for the aerodynamic simulation of H-Darrieus rotors. Energy 2015;90:680–90. https://doi.org/10.1016/j.energy.2015.07.102.

[55] Zhang T, Wang Z, Huang W, Ingham D, Ma L, Pourkashanian M. A numerical study on choosing the best configuration of the blade for vertical axis wind turbines. J Wind Eng Ind Aerodyn 2020;201:104162. https://doi.org/10.1016/j.jweia.2020.104162.

[56] Wekesa DW, Wang C, Wei Y, Danao LAM. Influence of operating conditions on unsteady wind performance of vertical axis wind turbines operating within a fluctuating free-stream: A numerical study. J Wind Eng Ind Aerodyn 2014;135:76–89. https://doi.org/10.1016/j.jweia.2014.10.016.

[57] Shukla DL, Mehta AU, Modi K V. Dynamic overset 2D CFD numerical simulation of a small vertical axis wind turbine. Int J Ambient Energy 2020;41:1415–22. https://doi.org/10.1080/01430750.2018.1517674.

[58] Subramanian A, Yogesh SA, Sivanandan H, Giri A, Vasudevan M, Mugundhan V, et al. Effect of airfoil and solidity on performance of small scale vertical axis wind turbine using three dimensional CFD model. Energy 2017;133:179–90. https://doi.org/10.1016/j.energy.2017.05.118.

[59] Sagharichi A, Maghrebi MJ, Arabgolarcheh A. Variable pitch blades: An approach for improving performance of Darrieus wind turbine. J Renew Sustain Energy 2016;8.

https://doi.org/10.1063/1.4964310.